



## Soot Particle Studies—Instrument Inter-Comparison—Project Overview

Eben S. Cross,<sup>1,2,\*</sup> Timothy B. Onasch,<sup>1,2</sup> Adam Ahern,<sup>1,2</sup> William Wrobel,<sup>1</sup> Jay G. Slowik,<sup>3</sup> Jason Olfert,<sup>4,12</sup> Daniel A. Lack,<sup>5,14</sup> Paola Massoli,<sup>2,5</sup> Christopher D. Cappa,<sup>6</sup> Joshua P. Schwarz,<sup>5</sup> J. Ryan Spackman,<sup>5</sup> David W. Fahey,<sup>5</sup> Arthur Sedlacek,<sup>4</sup> Achim Trimborn,<sup>2</sup> John T. Jayne,<sup>2</sup> Andrew Freedman,<sup>2</sup> Leah R. Williams,<sup>2</sup> Nga L. Ng,<sup>2</sup> Claudio Mazzoleni,<sup>7,13</sup> Manvendra Dubey,<sup>7</sup> Benjamin Brem,<sup>8</sup> Greg Kok,<sup>9</sup> R. Subramanian,<sup>9</sup> Steffen Freitag,<sup>10</sup> Antony Clarke,<sup>10</sup> Dwight Thornhill,<sup>11</sup> Linsey C. Marr,<sup>11</sup> Charles E. Kolb,<sup>2</sup> Douglas R. Worsnop,<sup>2</sup> and Paul Davidovits<sup>1</sup>

<sup>1</sup>*Chemistry Department, Boston College, Chestnut Hill, Massachusetts, USA*

<sup>2</sup>*Aerodyne Research, Inc., Billerica, Massachusetts, USA*

<sup>3</sup>*Chemistry Department, University of Toronto, Toronto, CA*

<sup>4</sup>*Brookhaven National Laboratory, Upton, New York, USA*

<sup>5</sup>*NOAA Earth System Research Laboratory, Chemical Sciences Division, Boulder, Colorado, USA*

<sup>6</sup>*Department of Civil and Environmental Engineering, University of California, Davis, California, USA*

<sup>7</sup>*Los Alamos National Laboratory, Los Alamos, New Mexico, USA*

<sup>8</sup>*Department of Civil and Environmental Engineering, University of Illinois, Urbana, Illinois, USA*

<sup>9</sup>*Droplet Measurement Technologies, Boulder, Colorado, USA*

<sup>10</sup>*Department of Oceanography, University of Hawaii, Honolulu, Hawaii*

<sup>11</sup>*Department of Civil and Environmental Engineering, Virginia Tech, Blacksburg, Virginia, USA*

<sup>12</sup>*Department of Mechanical Engineering, University of Alberta, Edmonton, Alberta, Canada*

<sup>13</sup>*Department of Physics, Michigan Technological University, Houghton, Michigan, USA*

<sup>14</sup>*Cooperative Institute for Research of the Environmental Sciences, University of Colorado, Boulder, Colorado USA*

*\*Now at the Department of Civil and Environmental Engineering, Massachusetts Institute of Technology, Cambridge, Massachusetts, USA*

Received 23 December 2009; accepted 6 March 2010.

This research was supported by the Office of Science (BER), Department of Energy (Atmospheric Science Program) grant No. DE-FG02-05ER63995 and the Atmospheric Chemistry Program of the National Science Foundation grants No. ATM-0525355 and ATM-0854916 to Boston College and Aerodyne Research, Inc. NOAA SP2 participation was supported by the NOAA Atmospheric Composition and Climate, and Health of the Atmosphere Programs, and the NASA Radiation Sciences Program and Upper Atmosphere Research Program. J. Olfert would like to thank Cambustion Ltd. for lending the Couette CPMA for this study. J. Olfert acknowledges the Goldhaber Distinguished Fellowship Program for providing funding for this project. C. Mazzoleni would like to thank MTU for start-up funds for SEM analysis and Owen P. Mills and Claire F. Drom at the Applied Chemical and Morphological Analysis Laboratory for their support.

Address correspondence to Eben Cross, Department of Civil and Environmental Engineering, Massachusetts Institute of Technology, Cambridge, MA 02139, USA. E-mail: escross@mit.edu

An inter-comparison study of instruments designed to measure the microphysical and optical properties of soot particles was completed. The following mass-based instruments were tested: Couette Centrifugal Particle Mass Analyzer (CPMA), Time-of-Flight Aerosol Mass Spectrometer—Scanning Mobility Particle Sizer (AMS-SMPS), Single Particle Soot Photometer (SP2), Soot Particle-Aerosol Mass Spectrometer (SP-AMS) and Photoelectric Aerosol Sensor (PAS2000CE). Optical instruments measured absorption (photoacoustic, interferometric, and filter-based), scattering (in situ), and extinction (light attenuation within an optical cavity). The study covered an experimental matrix consisting of 318 runs that systematically tested the performance of instruments across a range of parameters including: fuel equivalence ratio ( $1.8 \leq \phi \leq 5$ ), particle shape (mass-mobility exponent ( $D_{fm}$ ),  $2.0 \leq D_{fm} \leq 3.0$ ), particle mobility size ( $30 \leq d_m \leq 300$  nm), black carbon mass ( $0.07 \leq m_{BC} \leq 4.2$  fg) and particle chemical composition. In selected runs, particles were coated with sulfuric acid or dioctyl sebacate (DOS) ( $0.5 \leq \Delta r_{ve} \leq 201$  nm) where  $\Delta r_{ve}$  is the change in the volume equivalent radius due to the coating material.

**The effect of non-absorbing coatings on instrument response was determined. Changes in the morphology of fractal soot particles were monitored during coating and denuding processes and the effect of particle shape on instrument response was determined. The combination of optical and mass based measurements was used to determine the mass specific absorption coefficient for denuded soot particles. The single scattering albedo of the particles was also measured. An overview of the experiments and sample results are presented.**

---

[Supplementary materials are available for this article. Go to the publisher's online edition of *Aerosol Science and Technology* to view the free supplementary files.]

## 1. INTRODUCTION

Soot particles that contain black carbon (BC) are emitted during combustion of fossil and biomass fuels. Air borne aerosol particles containing BC directly absorb sunlight, heating the particles and the surrounding atmosphere (Schwartz and Buseck 2000). Most other aerosol particles predominately scatter sunlight cooling the surface and lower atmosphere (Ramanathan et al. 2001). It has been estimated that the direct radiative effect of BC is the second-most important contributor to global warming after absorption by CO<sub>2</sub> (Jacobson 2001). Ongoing studies continue to underscore the climate forcing importance of BC (Ramanathan and Carmichael 2008; Grieshop 2009; Rypdal 2009; Ramanathan and Feng 2009). However, estimates of BC climate effects are highly uncertain in large part because of the physical and chemical complexity of particles containing BC.

Freshly emitted soot particles are typically fractal hydrophobic aggregates consisting of black carbon spherules with diameters in the range of ~20–40 nm (Seinfeld and Pandis 2006; Chakrabarty et al. 2009). This complex morphology makes quantitative measurement of BC particle properties particularly challenging (Park et al. 2003; Chakrabarty et al. 2006). Fractal BC cores are often coated with aliphatic organic compounds from lubricating oil and unburned fuel (Canagaratna et al. 2004; Sakurai et al. 2003; Kittelson 1998) as well as polycyclic aromatic hydrocarbons (PAHs) (Marr et al. 2004; Jiang et al. 2005), depending on the fuel content and combustion conditions. Sulfuric acid has also been detected in diesel and aircraft-emitted soot particles (Curtius et al. 1998; Onasch et al. 2009). With increasing atmospheric residence time, soot particles acquire additional coatings through deposition of semivolatile atmospheric species or coagulation with pre-existing particles. Such processes transform the morphological, chemical and optical properties as well as the cloud condensation nuclei (CCN) activity, of the soot particles, further complicating parameterization of their climate effects. To fully characterize BC-containing particles one must measure, in real-time, the mass of BC in the particles as well as the optical properties (absorption, scattering, and extinction) of the particles.

The recent development of aerosol mass spectrometers now allows real-time determination of the size and composition of

aerosol particle ensembles (Murphy 2006; Canagaratna et al. 2007). Instruments have also been developed to provide real-time measurements of the mass and optical properties of BC-containing particles. Some mass-based instruments include the Single Particle Soot Photometer (SP2) (Stephens et al. 2003; Schwarz et al. 2006) and the Couette Centrifugal Particle Mass Analyzer (CPMA) (Olfert and Collings 2005). Common techniques for aerosol optical property measurements include: cavity ring down spectroscopy (Smith and Atkinson 2001; Bulatov et al. 2002; Atkinson 2003; Strawa et al. 2003; Pettersson et al. 2004; Moosmüller et al. 2005) for aerosol extinction; nephelometry (Heintzenberg and Charlson 1996 and references therein) for aerosol scattering; photo-acoustic (Arnott et al. 1999; Lack et al. 2006), interferometry (Davis 1980; Campillo and Lin 1981; Fluckiger et al. 1985) and real-time filter-based methods such as the aethalometer (Hansen et al. 1984), particle soot absorption photometer (PSAP) (Bond et al. 1999) and multi angle absorption photometer (MAAP) (Petzold et al. 2004) for aerosol absorption. Combining measurements from these instruments has the potential to provide real-time/near real-time quantitative physical, chemical and optical characterization of BC-containing aerosol particles. To achieve this potential, instrument performance must be validated using a wide range of BC-containing particles with known properties.

Inter-comparison studies under controlled conditions (known particle mass, size, number and composition) are an indispensable step in the instrument validation process. Inter-comparison measurements are necessary if one is to attain the degree of understanding required to reduce the large uncertainties associated with the effects of BC-containing aerosol particles on climate.

Several previous inter-comparison studies of BC measurements have been conducted (Slowik et al. 2007a and references therein). Two inter-comparison studies have been completed in Boston College laboratories, one in May 2005 (Slowik et al. 2007a) and another in July of 2008—the subject of the present article. The key component of the Boston College laboratory apparatus is a well-characterized soot generation/sampling system developed by the Boston College/Aerodyne Research, Inc., group (Slowik et al. 2007a). The soot particle generation/sampling source used in the current inter-comparison study is improved relative to our previous work. The improved system is capable of providing stable, monomodal soot distributions across a size range of  $30 \leq d_m \leq 300$  nm. The new soot sampling system is also able to provide a significantly higher total particle flow making it possible to simultaneously measure properties of soot particles with up to 18 instruments (total flow rate ~22 L/min).

Twenty-six scientists representing 12 institutions participated in the inter-comparison study operating 7 mass-based and 9 optically based instruments; filter samples for Scanning Electron Microscopy (SEM) and Organic Carbon Elemental Carbon (OCEC) analyses were also obtained. The study covered an experimental matrix consisting of 318 runs that systematically tested the performance of instruments across a wide range of

parameters including: fuel equivalence ratio ( $1.8 \leq \phi \leq 5$ ), particle shape (mass-mobility exponent  $2.0 \leq D_{fm} \leq 3.0$ ), particle mobility size ( $30 \leq d_m \leq 300$  nm), black carbon mass ( $0.07 \leq m_{BC} \leq 4.2$  fg) and particle chemistry and density (changed via coatings). In select runs, particles were coated with a known thickness of sulfuric acid or dioctyl sebacate (DOS) ( $0.5 \leq \Delta r_{ve} \leq 201$  nm).

Highlights of the inter-comparison study include: CPMA mass measurements of coated soot particles and their corresponding soot cores, SMPS-AMS/CPMA total mass measurement comparisons, multiple measurements of the mass specific absorption coefficient for different types of soot particles, mass specific absorption enhancement ( $E_{abs}$ ) as a function of coating type and thickness, wavelength-dependent measurements of absorption, scattering, and extinction as a function of soot particle type, and particle shape determination as a function of fuel-to-air ratio. Collapse of particle shape was observed in the coating-denuding process. In addition to flame-generated soot, black carbon particles obtained by atomizing fullerene soot, oxidized flame soot, Regal black toner, and Aquadag paint were also characterized. In this article, we only present results obtained for flame-generated soot particles. The intent of the article is to explain the goals of the study, to provide an overview of the experimental methodology, and to illustrate the type of data obtained by presenting key sample results for selected instrument inter-comparison experiments. Accordingly, descriptions of the specific instruments are restricted to providing the basic operating principles necessary to understand the nature and range of information a given instrument can provide and what aspects of the data provided can be meaningfully inter-compared with other instruments. More detailed results and discussions related to specific instruments will be provided in subsequent publications.

## 2. INTER-COMPARED INSTRUMENTS AND SCOPE OF THE STUDY

We divide the instruments tested into two categories: mass-based and optically-based, listed in Tables 1a and 1b, respectively. Mass-based instruments measure parameters that are directly or computationally related to particle mass. Here, empirical inter-comparison of mass-based instruments utilizing different measurement principles address instrument calibration and performance. The optically-based instruments measure absorption, scattering, and/or extinction of the particle ensemble at specified wavelengths. As shown in Table 1b, the optical instruments covered a wavelength range of  $\lambda = 355$  nm–1064 nm. Inter-comparisons of measurements obtained at the same wavelength provide a means for diagnosing instrument-to-instrument variability. Comparing optical measurements obtained across a range of wavelengths provides insight into the wavelength dependence of the scattering, absorption, and extinction for different types of soot particles.

Tables 1a and 1b include the name, abbreviation and manufacturer of each instrument, a brief description of the measurement provided and units for the key measured parameter. Key

instruments used to characterize and continuously monitor the soot particles are listed in Table 1c. Results from instruments marked with an asterisk are not included in the present article and will be presented in subsequent publications.

The SP2 and LS-ToF-AMS mass-based instruments can provide single particle information. In this study, the CPMA and SP2 instruments report information on a mode-specific basis (i.e., particles that are singly or doubly charged in the DMA), the optically-based instruments measure ensemble average absorption, scattering, and extinction ( $\beta_{abs}$ ,  $\beta_{sca}$ , and  $\beta_{ext}$ ). Because in the inter-comparison experiments discussed here, the particles are well characterized with respect to size ( $d_m$ ) and concentration (particles/cm<sup>3</sup>) per-particle absorption, scattering and extinction cross sections ( $\sigma_{abs}$ ,  $\sigma_{sca}$ , and  $\sigma_{ext}$ ) can be obtained. To minimize the influence of multiply-charged particles on the measured cross-sections, all ensemble-based data shown in the article have a number fraction of singly charged particles  $\geq 0.93$ .

Coupled measurements of absorption and scattering (i.e., PASS-3) or absorption and extinction (i.e., PAS and CRD-AES) allow determination of the single scattering albedo (SSA) of the sampled aerosol particles. Equations (1a) and (1b) show the relationship between SSA and the measured cross-sections ( $\sigma_{sca}$ ,  $\sigma_{abs}$ ,  $\sigma_{ext}$ )

$$SSA = \sigma_{sca}/(\sigma_{sca} + \sigma_{abs}) \quad [1a]$$

$$SSA = (\sigma_{ext} - \sigma_{abs})/\sigma_{ext} \quad [1b]$$

Single scattering albedo (SSA) values vary from near zero for black, completely absorbing aerosol particles to  $SSA = 1$  for a non-absorbing aerosols.

Soot particles were produced at controlled fuel-to-air equivalence ratios in the range  $\sim\phi = 2$  to  $\phi = 5$ . Experiments were conducted with (1) nascent soot particles (where the condensed organic material from the flame is present on the BC core surface), (2) nascent — denuded soot particles (primarily BC core only), (3) soot particles coated with sulfuric acid or DOS, and (4) coated and then denuded soot particles.

Of the instruments tested, the SP-AMS and CPMA are recently developed mass-based instruments and the PTI, PASS-3, and CAPS are newly developed optically-based instruments. For these instruments the present inter-comparison experiments provide the first wide-ranging operational test with fully characterized soot particles. Brief descriptions of the instruments used in the inter-comparison study are provided in the supplemental information.

## 3. EXPERIMENTAL ARRANGEMENT

### 3.1. Particle Generation

The re-designed soot generation/sampling system is shown in Figure 1. The arrangement of the apparatus varies somewhat with specific experiments. As in our first inter-comparison study (Slowik et al. 2007), soot particles are produced with a McKenna flat flame burner by the combustion of a mixture of C<sub>2</sub>H<sub>4</sub>



TABLE 1b  
Optically Based Instruments

Instrument	Measurement Obtained	Measure	Unit
Photoacoustic Spectrometer (PAS) [NOAA CSD]	Absorption coefficient determined from measurement of the pressure waves created by heating the particles with a modulated laser source ( $\lambda = 532$ nm)	$\beta_{abs}$	$Mm^{-1}$
Photoacoustic Soot Spectrometer (PASS-3) [Droplet Measurement Technology]	Similar to the PAS in principle, the PASS-3 measures thermal expansion at three wavelengths ( $\lambda = 405, 532,$ and $781$ nm). The instrument is also equipped with a scattering sensor for each $\lambda$ based on reciprocal nephelometry	$\beta_{abs}$ $\beta_{sca}$	$Mm^{-1}$ $Mm^{-1}$
Photo-Thermal Interferometer (PTI) [BNL]	Absorption coefficient of a particle based on the change in refractive index of an excited particle's proximal gases ( $\lambda = 532$ nm)	$\beta_{abs}$	$Mm^{-1}$
Cavity Ring Down Aerosol Extinction Spectrometer (CRD-AES) [NOAA CSD]	Extinction coefficient of particles in an optical cavity ( $\lambda = 355, 532,$ and $1064$ nm) and as a function of RH	$\beta_{ext}$	$Mm^{-1}$
Cavity Attenuated Phase Shift Extinction Monitor (CAPS) [Aerodyne Research, Inc.]	Similar to the CRD-AES, CAPS measures extinction at ( $\lambda = 445 \pm 8$ nm)	$\beta_{ext}$	$Mm^{-1}$
<sup>a</sup> Multi-Angle Absorption Photometer (MAAP) [ThermoElectron]	Absorption coefficient determined from the change in transmitted light ( $\lambda = 670$ nm) through a filter. Corrections applied for aerosol scattering and specific instrument geometry	$\beta_{abs}$	$Mm^{-1}$
<sup>a</sup> Particle Soot Absorption Photometer (PSAP) – 2 in number [Radiance Research.]	Absorption coefficients measured at $\lambda = 470, 530,$ and $660$ nm	$\beta_{abs}$	$Mm^{-1}$
<sup>a</sup> Nephelometer [TSI]	Scattering coefficients at $\lambda = 450$ nm, $550$ nm, and $700$ nm.	$\beta_{sca}$	$Mm^{-1}$

<sup>a</sup>Results not included in the present article and will be presented in subsequent publications.

TABLE 1c  
Particle Characterization and Monitoring Instrumentation

Instrument	Measurement Description	Measure	Unit
Condensation Particle Counter (CPC) – 3 in number [TSI]	Concentration of aerosol particles using condensation-growth and light scattering.	$N_{CN}$	$\#/cm^3$
Differential Mobility Analyzer (DMA) – 2 in number [TSI]	Size-selects the aerosol distribution by balancing electrostatic and drag forces on a charged particle distribution providing particles of known mobility diameter	$d_m$	nm
<sup>a</sup> Cloud Condensation Nuclei Counter (CCN) [Droplet Measurement Technology]	Concentration and cloud nuclei potential of aerosols. Determination of the critical supersaturation ( $SS_c$ ) the supersaturation at which 50% of the particles activate to cloud droplets	$N_{CCN}, SS_c$	$\#/cm^3$
<sup>a</sup> Diffusion Charger (DC2000CE) [EcoChem Analytics]	Active surface area of the particles in millimeters squared per cubic meter measured by diffusion charging	$mm^2/m^3$	$mm^2/m^3$

<sup>a</sup>Results not included in the current article and will be presented in subsequent publications.

(ethylene) and O<sub>2</sub> premixed with a dilution flow of N<sub>2</sub> and surrounded by a sheath flow of N<sub>2</sub>. In the new setup, the base of the burner is mounted on an  $x - y - z$  translation stage and the combined soot generation/sampling apparatus is secured within a stainless steel frame attached to an optical table. This arrangement provides a stable reproducible alignment of the sampling inlet with the soot source. The figure also shows the arrangement for producing black carbon particles by atomization of aqueous suspensions.

After generation, particles are size-selected with a Differential Mobility Analyzer (DMA; TSI model 3080—calibrated and operated with a sheath flow of N<sub>2</sub>). The improved alignment control allows the optimization of the width and peak position of the polydisperse soot distribution. As a result, the DMA can be set to select a size that corresponds to the falling edge of the polydisperse distribution thereby providing monodisperse distributions of soot particles with minimal influence from multiply charged particles. Through characterization experiments, the optimal sampling height (distance between the burner surface and sampling inlet) was established to be  $\sim 8''$ .

In Figure 2 we show examples of typical number distributions of nascent size-selected soot particles produced at a fuel equivalence ratio  $\phi = 2.0 \pm 0.2$  ( $d_m = 31$  nm,  $d_m = 97$  nm, and  $d_m = 276$  nm). The 1-sigma width of the  $d_m$  size distribution is approximately  $\pm 20\%$  controlled by the 5:1 ratio of sheath to sample flow in the DMA. Periodic monitoring of the voltage setting and flows in the DMA indicated that the mode  $d_m$  size of a typical run is stable to within 2%. The size distributions shown have less than 5% of the particle number attributed to multiply charged particles. The number fraction of singly charged particles for each experimental run was calculated from the logged SMPS number distributions and found to be in excellent agreement (within 2%) with the q1 number fraction measured with the SP2 and LS-ToF-AMS instruments. The scales for the three distributions are different as indicated by each verticle axis.

### 3.2. Flow Control and Sampling

Sensitivities of the instruments in this study vary. For accurate measurement, each instrument requires a particle number concentration in a specific range. The inter-comparison study included instruments that measure single particle properties and instruments that measure ensemble average properties. Typically, instruments that measure ensemble average properties require flows with number concentrations in the range  $\sim 1,000$ – $50,000$  p/cm<sup>3</sup> (dependent on particle size) while single particle instruments are most effective at concentrations of  $\sim 100$ – $3,000$  p/cm<sup>3</sup>. Therefore, careful control of the number concentration of soot particles is essential. Flow meters, flow controllers and humidity monitors (not shown in Figure 1) were used to define, control and monitor the flows and resulting soot number concentrations throughout the inter-comparison study. All input flows to the soot source (fuel, oxygen, pre-mix nitrogen and sheath nitrogen) were carefully monitored to ensure the stability of the

system for each equivalence ratio tested.

As indicated in the inset of Figure 1, a flow of N<sub>2</sub> (called “dilution N<sub>2</sub> flow”) is introduced around the sampling tip to prevent soot from clogging the inlet. The dilution N<sub>2</sub> flow also allows control and adjustment of the total soot particle concentration in accord with the requirements of the sampling instrumentation. By systematically varying the dilution N<sub>2</sub> flow in the soot-particle sampling inlet, particle number concentrations were obtained over the desired range. The majority of the experimental runs were obtained with soot particle number concentrations between  $1000$ – $4000$  p/cm<sup>3</sup>.

An important modification to the soot generation/sampling system was the installation of a diaphragm pump downstream of the DMA (not shown in Figure 1). The diaphragm pump is used to produce a sample flow rate of  $\sim 2$  L/min through the DMA ( $\sim 5:1$  sheath: sample), keeping the size resolution of the DMA high ( $\pm 20\%$  of the  $d_m$  mode diameter). Tests with and without the diaphragm pump integrated into the sampling line confirmed that the pump did not affect the chemical or physical properties of the soot particles across the range of  $d_m$  sizes and equivalence ratios tested in the inter-comparison study. To increase the total flow of the system to the desired 22 L/min, an additional N<sub>2</sub> dilution flow was incorporated into the system downstream of the DMA and the coating/denuding apparatus. This arrangement also allowed humidification of the additional N<sub>2</sub> flow and subsequent relative humidity (RH) control within the plenum.

After appropriate dilution and processing (if coated and/or denuded) the particles flow into the plenum chamber. From the plenum, the flows are distributed to the various instruments listed in Tables 1a–1c (described in greater detail in the supplemental information). At various points during the inter-comparison the number concentration of soot particles was monitored at each of the exit lines from the sampling plenum to confirm that no sampling biases were present.

### 3.3. Coating and Denuding Apparatus

In the coating and/or denuding experimental runs, the particles are passed through the requisite sections of the apparatus (Figure 1). The coating section consists of a 36'' long 3/8'' diameter quartz tube with two ( $\sim 12''$  in length) heating stages referred to as T1 and T2. Throughout the experiments, T1 was typically held  $\sim 30^\circ\text{C}$  warmer than T2 with T1 temperatures ranging from  $60$ – $140^\circ\text{C}$ , depending on the coating thickness required for each experimental condition. The coating material of interest (either DOS or H<sub>2</sub>SO<sub>4</sub>) was contained within a small reservoir located in the first heated section. The last 12'' section of the coating tube was kept at room temperature. As shown in Figure 1, two H<sub>2</sub>SO<sub>4</sub> coating reservoirs were available, one was located upstream of the DMA and a second located downstream of the DMA. The upstream reservoir was used to coat the polydisperse distribution of soot particles. In this case, coated soot particles were then size selected with the DMA. In contrast, the downstream reservoir coated size-selected soot particles.

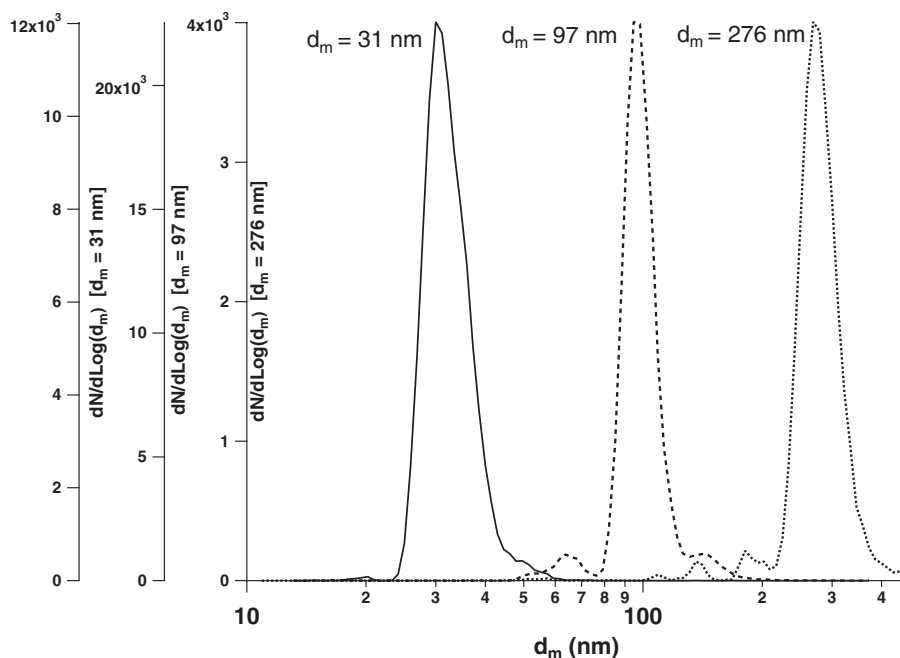


FIG. 2. Three particle size distributions provided by the DMA set to size-selected mobility diameters  $d_m = 31$  nm,  $d_m = 97$  nm, and  $d_m = 276$  nm obtained at a fuel equivalence ratio  $\phi = 2.0 \pm 0.2$ . The integral under each curve provides the number concentration ( $\text{p}/\text{cm}^3$ ) between the limits of integration.

The combined information obtained with the CPMA, SP-AMS, LS-ToF-AMS, and SMPS is illustrated in Figure 3 to demonstrate measurements of both the refractory and non-refractory content of the soot particles. In Figures 3a and b we show the physical and chemical characterization of soot particles before and after coating with DOS. The upper panel of Figure 3 shows the normalized number concentration of the particles measured with the CPMA as a function of the CPMA voltage. The voltage obtained from the mode of a log-normal fit to the CPMA data is used to determine the particle mass. The CPMA sample flow rate was held constant at 0.3 L/min during the experiments and the rotational speed was varied with particle size to maintain optimal mass resolution across the range of conditions studied. Specifically,  $\lambda_{\text{CPMA}}$ , a dimensionless number that quantifies the CPMA mass resolution was kept within a range from  $-0.3 \leq \lambda_{\text{CPMA}} \leq -0.1$  (see equation 13 in Olfert and Collings 2005). The middle panel shows the measured chemical ion signals as a function of their measured vacuum aerodynamic diameter. For the nascent soot core, the chemical ion signals for  $m/z = 36$  (refractory BC signal) measured with the SP-AMS is shown. For the DOS-coated condition, the  $m/z = 36$  (from the SP-AMS) and  $m/z = 185$  (non-refractory organic signature of DOS measured with the LS-ToF-AMS) are shown. The bottom panel of the figure shows the volume distributions measured with the SMPS instrument showing the change in mobility diameter as a result of the DOS coating.

The thermal denuder, designed and characterized by Aerodyne Research Inc. in collaboration with the University of Colorado (Huffman et al. 2008) consists of a 22'' heated section held

at 250°C followed by a 24'' section of activated charcoal kept at room temperature. As particles pass through the heated region, the non-refractory components on the particles vaporize and are then adsorbed by the activated charcoal. As a result, for this study, the operational definition of “non-refractory material” is matter that is removed from the particles at 250°C in the denuder. Likewise, refractory material is that which remains in the particle phase after passing through the denuder. Experimentally, the particles transmitted through the denuder are the black carbon cores generated under the specific experimental condition. The composition of the denuded soot particles was confirmed with the LS-ToF-AMS by the absence of measurable chemical ion signals due to non-refractory material during denuded particle runs. The denuder was used to systematically examine the size ( $d_m, d_{va}$ ), mass-mobility exponent ( $D_{fm}$ ), and mass of the BC core for each condition tested: Nascent soot ( $2.0 \leq \phi \leq 5.0$ ), DOS-coated soot ( $\phi = 2.0 \pm 0.2$ ), and  $\text{H}_2\text{SO}_4$ -coated soot ( $\phi = 2.0 \pm 0.2$ ). That is, for a given ‘coated’ experimental run, there is a corresponding denuded experimental run.

#### 4. EXPERIMENTAL OBJECTIVES AND SELECTED RESULTS FOR MASS-BASED INSTRUMENTS

##### 4.1. Couette Centrifugal Particle Mass Analyzer (CPMA)

In conjunction with the DMA and CPC instruments, the CPMA provides the most direct, shape-independent measure of particle mass (Olfert and Collings 2005). To illustrate the utility of the CPMA measurements we (a) validated the calibration of the CPMA with polystyrene latex spheres (PSL) of known

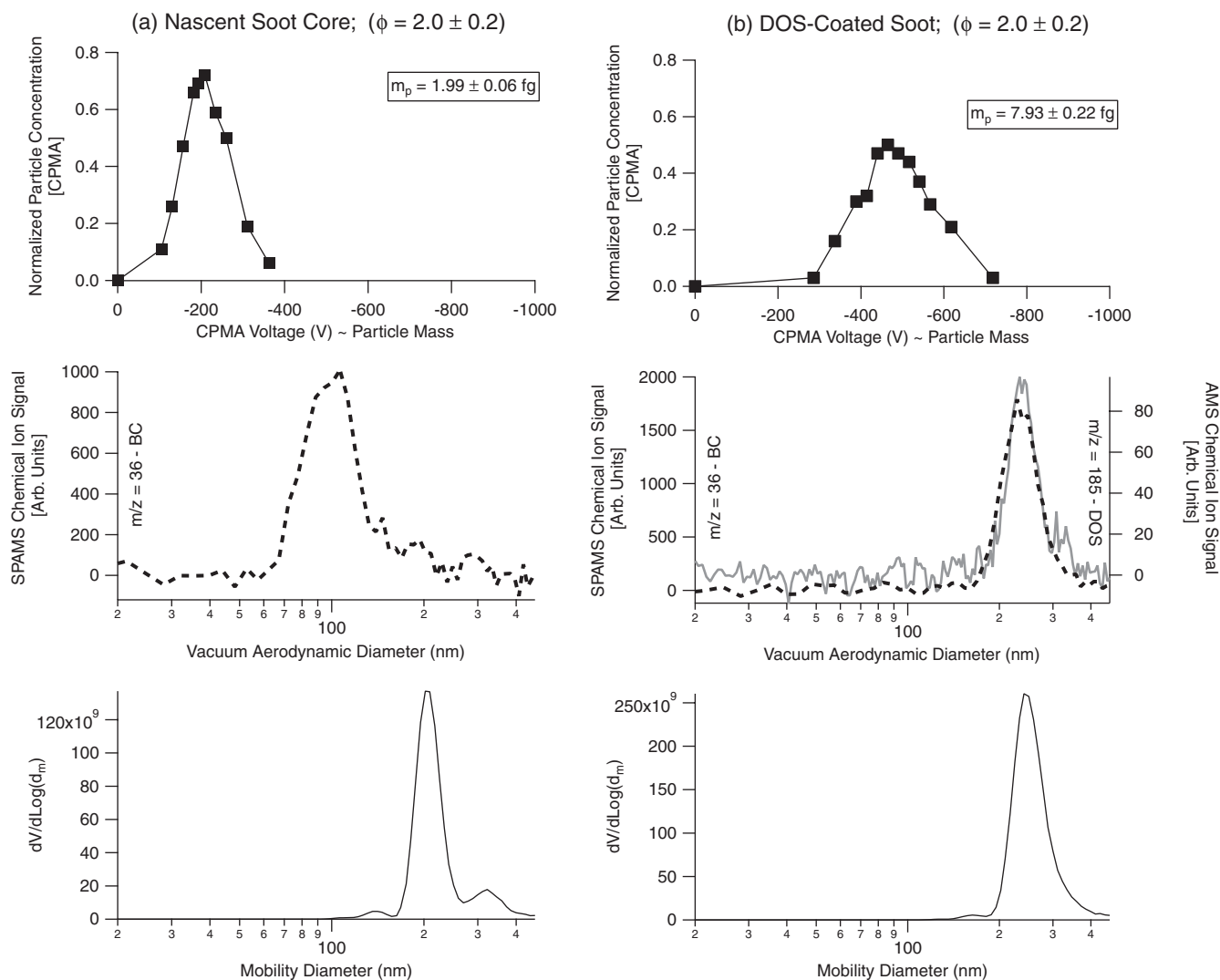


FIG. 3. Measured CPMA (upper panel), vacuum aerodynamic (middle panel) and mobility (lower panel) distributions for (a) an uncoated nascent soot core ( $\phi = 2.0 \pm 0.2$ ) and (b) the same soot core coated with DOS.

diameter and density, (b) used the CPMA-measured mass ( $m_p$ ) of nascent and denuded soot runs to determine the mass fraction of black carbon in soot particles produced at different equivalence ratios, (c) used the CPMA-measured mass in conjunction with the known  $d_m$  to determine the mass-mobility exponent of soot particles produced at different fuel equivalence ratios, and (d) monitor changes in the morphology of coated and denuded soot particles.

#### 4.1.1. Calibration

In Figure 4 we show the CPMA-determined particle mass for commercially manufactured PSL particles (Duke Scientific, Corp.) as a function of the calculated mass (based on the known density  $\rho = 1.054$  g/cm<sup>3</sup> and diameter ( $d_p$ ) of the PSL particles.

The CPMA-measured PSL particle mass is in good agreement with the calculated PSL mass across a mass range of  $m_p =$

0.1–120 fg. The error bars shown in the CPMA measured mass axis correspond to the 1-sigma width of the log-normal fit to the mass distribution obtained with the CPMA.

#### 4.1.2. Black carbon mass content of soot particles

During the inter-comparison studies, experimental runs with nascent and/or coated soot particles were coupled with corresponding denuded soot runs. In this way, the size, shape and mass of the refractory BC core were characterized after the condensed phase organic or inorganic material was removed.

With the CPMA measurement, nascent soot runs coupled with corresponding denuded runs provide a measure of the mass fraction of BC in the nascent soot produced at different fuel equivalence ratios ( $\phi$ ). Figure 5 displays the CPMA-measured mass for nascent soot (y axis) versus the CPMA-measured mass for the corresponding denuded soot particles. Measurements shown in the figure were obtained for soot particles produced

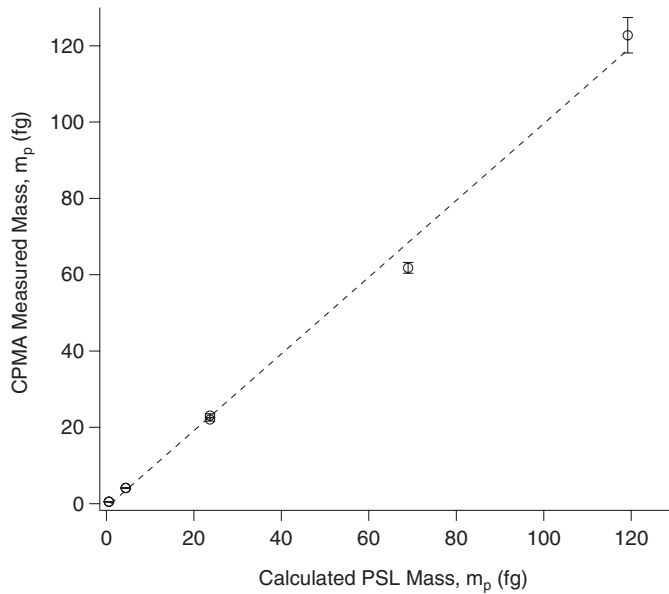


FIG. 4. CPMA-measured mass for commercially manufactured PSL particles as a function of calculated particle mass (via density and size). Linear regression fit to the data yields a slope of 1.01 and  $R^2 = 0.998$ .

at equivalence ratio of  $\phi = 2.0 \pm 0.2$  (grey crosses) and  $\phi = 5.0 \pm 0.2$  (black circles). The range of mass values displayed was obtained by varying the mobility size ( $d_m$ ) of the particles.

The results in Figure 5 show that the BC mass fraction of soot particles produced at  $\phi = 2.0 \pm 0.2$  is on average 0.74 while soot produced at  $\phi = 5.0 \pm 0.2$  has a BC mass fraction of 0.32. The lower BC mass fraction of soot particles produced at the high (i.e., fuel rich) equivalence ratios is consistent with incomplete combustion producing more condensable organics (aliphatic and PAH) within the flame that subsequently coat the refractory BC core.

#### 4.1.3. Measurement of particle mass-mobility exponent

The mass-mobility exponent ( $D_{fm}$ ) is obtained from the relationship between the measured mass ( $m_p$ ) and mobility diameter ( $d_m$ ) of the soot particles via equation 2 (Park et al. 2004):

$$m_p = C \cdot d_m^{D_{fm}} \quad [2]$$

where  $C$  is a proportionality constant and  $D_{fm}$  yields the power law dependence between the particle mass and the hydrodynamic length scale. The mass-mobility exponent has previously been referred to as the mass fractal dimension (Kim et al. 2009) and is analogous (although not necessarily equivalent) to the fractal dimension. In the present study, the mass-mobility exponent is used to measure changes in the morphology of nascent, denuded and coated soot particles.

For the results presented here, the CPMA provides a direct measure of  $m_p$ , and for a given series of experimental runs over which  $d_m$  was varied and the soot particle type (i.e., equivalence ratio) was held constant,  $D_{fm}$  can be determined. Figure

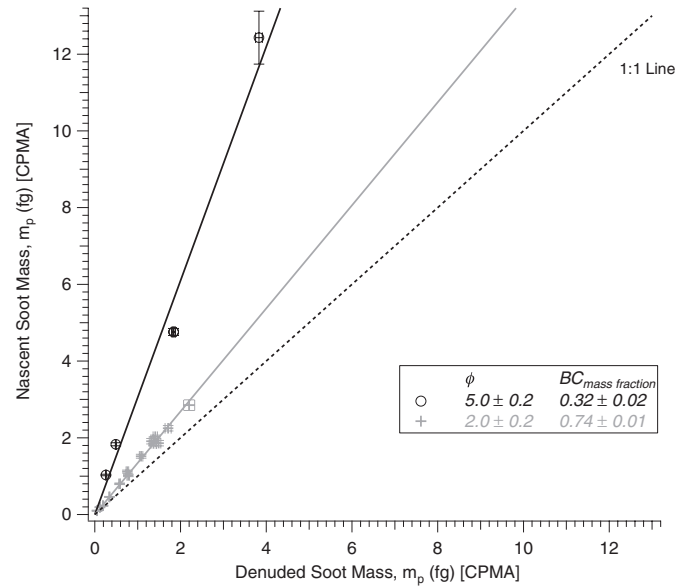


FIG. 5. CPMA-measured mass for nascent soot particles (y-axis) plotted as a function of the CPMA-measured mass for the corresponding denuded soot particles (x-axis). That is, soot particles having the same refractory core are compared before and after denuding. The error bars shown correspond to the  $1\sigma$  standard deviation in the CPMA mass measurement.

6 shows a plot of the CPMA-measured mass as a function of the selected  $d_m$  for nascent soot particles produced at  $\phi = 2.0 \pm 0.2$  (grey open symbols) and  $\phi = 5.0 \pm 0.2$  (black solid circles). The dashed lines in the figure are linear fits to the data and indicate that nascent soot produced at  $\phi = 2.0 \pm 0.2$  has a  $D_{fm} = 2.24 \pm 0.03$  (fractal aggregate) whereas the nascent soot produced at  $\phi = 5.0 \pm 0.2$  has a  $D_{fm} = 3.04 \pm 0.04$  (near-spherical). This observation is consistent with the significantly larger non-BC mass fraction ( $\sim 0.74$ ) of the  $\phi = 5.0$  soot particles compared to the  $\phi = 2.0$  soot particles shown in Figure 5. We note that the mass-mobility exponents reported here represent the ensemble average  $D_{fm}$  for each type of soot particle produced.

As is evident in Figure 6, the two linear fits shown do not have the same intercept ( $C'$ ) value and appear to cross at  $d_m \sim 60$  nm. This phenomenon is the result of differences between  $N_{pp} > 60$  vs.  $N_{pp} < 60$  regimes (DeCarlo et al. 2004). The fractal dimension (or mass-mobility exponent) is higher for  $N_{pp} < 60$ . This is obvious for the extreme case; for a particle with  $N_{pp} = 1$ ,  $D_{fm} = 3$ . Likewise, an aggregate of 2 spherules must have the most compact possible shape. However, as more spherules are added, the length scale grows more rapidly with respect to  $N_{pp}$ , eventually approaching the  $N_{pp} > \sim 60$  limit. In other words, soot particles are not true fractals in the mathematical sense: their self-similarity does not hold across infinite length scales, and breaks down in the limit of small  $N_{pp}$ .

Within experimental uncertainties, the relationship between  $\log(m_p)$  and  $\log(d_m)$  is well described by a linear fit. Size-dependent changes in either  $C'$  or  $D_{fm}$  would be expected to

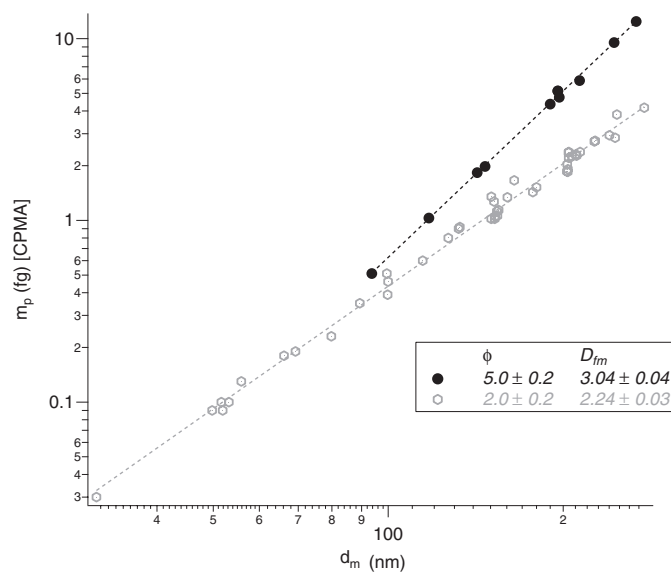


FIG. 6. CPMA-measured particle mass for nascent soot particles produced at  $\phi = 2.0 \pm 0.2$  and  $\phi = 5.0 \pm 0.2$  as a function of mobility diameter. Fits shown as the dashed lines indicate that the low equivalence ratio soot particles are fractal-like with a  $D_{fm} = 2.24 \pm 0.03$  whereas the high equivalence ratio soot particles are near-spherical with a  $D_{fm} = 3.04 \pm 0.04$ .

appear as a change in slope of the line, which is not observed for the size range studied. From this observation, we conclude that within uncertainties in our measurements, the data are well represented by a size-independent  $D_{fm}$  value.

#### 4.1.4. Effect of coating-denuding process on soot particle re-arrangement

To explore whether the fractal soot particles undergo re-arrangement as a result of the coating-denuding process we measured the mass-mobility exponent of the particles at each stage of the coating-denuding process. In Figure 7a we show the plot of  $m_p$  versus  $d_m$  for DOS-coated and DOS-coated-denuded soot particles produced at  $\phi = 2.0 \pm 0.2$ . In Figure 7b we show a similar plot for  $H_2SO_4$ -coated and  $H_2SO_4$ -coated-denuded particles. The dashed line shown in each plot represents the mass-mobility relationship for nascent-denuded  $\phi = 2.0 \pm 0.2$  soot particles that have not been coated with either DOS or  $H_2SO_4$ . The slope of the dashed line ( $D_{fm} = 2.12 \pm 0.04$ ) represents the mass-mobility exponent of nascent-denuded soot particles produced at  $\phi = 2.0 \pm 0.2$ .

The coating mass fractions ranged from  $\sim 0.40$ – $0.99$  for the data shown in Figures 7a and 7b. The data show, that across this range of coating mass fractions, the coated soot particles (either DOS or  $H_2SO_4$ ) have a  $D_{fm} \sim 3$  (near-spherical). The DOS-coated-denuded soot particles shown in Figure 7a retain their fractal aggregate shape with a measured  $D_{fm} = 2.17 \pm 0.06$ . However, the  $H_2SO_4$ -coated-denuded soot particles, shown in Figure 7b, have a  $D_{fm} = 2.49 \pm 0.08$  indicating that the  $H_2SO_4$ -coating-denuding process has caused the soot parti-

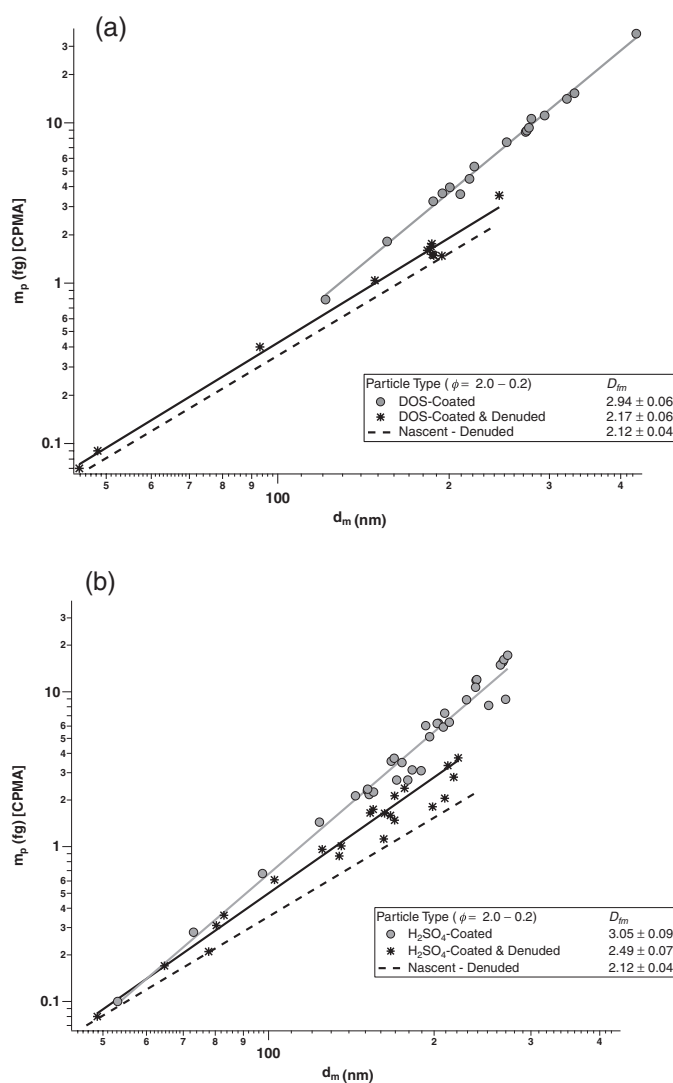


FIG. 7. CPMA-measured  $m_p$  as a function of the  $d_m$  for (a) DOS-coated & DOS-coated-denuded soot runs and (b)  $H_2SO_4$ -coated &  $H_2SO_4$ -coated-denuded soot runs. In all runs shown, original soot cores were produced at  $\phi = 2.0 \pm 0.2$ . For reference, the dashed line in each plot shows the  $D_{fm} = 2.12 \pm 0.04$  measured for nascent-denuded soot particles.

cles to undergo re-arrangement toward a more compact shape (from  $D_{fm} = 2.12$  to  $D_{fm} = 2.49$ ).

A pictorial view of the coating-denuding process is displayed with sample SEM images shown in Figure 8. The figure includes an SEM image for (a) a nascent soot particle; (b) a DOS-coated-denuded soot particle, and (c) a  $H_2SO_4$ -coated-denuded soot particle. In all three cases the original soot particles were generated at  $\phi = 2.0 \pm 0.2$  and size selected at  $d_m = 209$  nm. The large black regions are holes in the SEM filter surface to allow sufficient gas flow for impaction. These images are consistent with the data displayed Figures 7a and b. The  $H_2SO_4$  coating causes the fractal soot core to collapse to a more compact shape whereas the DOS coating does not appear to influence nearly as strongly the fractal nature of the

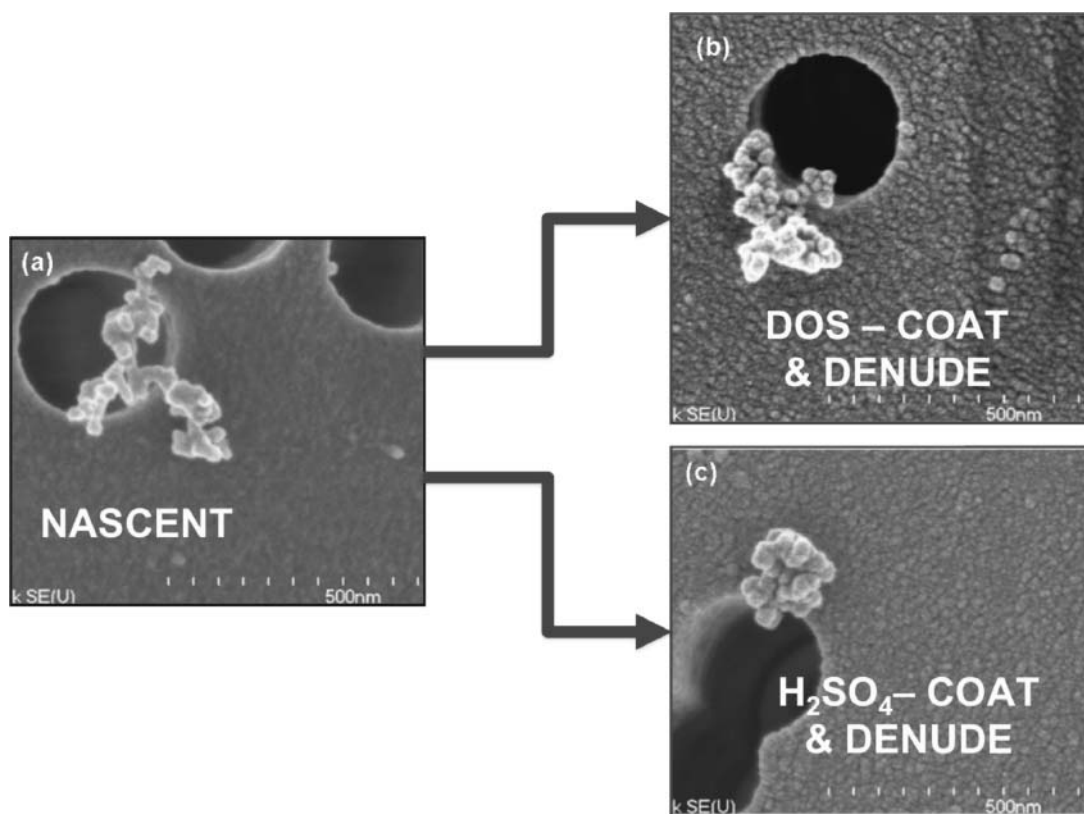


FIG. 8. SEM images showing the effect of the coating/denuding process for fractal soot particles generated at  $\phi = 2.0 \pm 0.2$  with an original mobility diameter of  $d_m = 209$  nm; (a) nascent soot particle; (b) DOS-coated then denuded soot particle, and (c)  $\text{H}_2\text{SO}_4$ -coated then denuded soot particle. The dark circles are holes that are part of the particle collecting polycarbonate membrane. The images were collected using a Hitachi S-4700 field emission scanning electron microscope. Before imaging, the filters were coated with platinum. The visible granularity of the background in some of the images is due to the platinum coating.

original soot core. The observation of soot particle collapse as a result of the  $\text{H}_2\text{SO}_4$ -coating-denuding process is consistent with the observations of Zhang et al. (2008) and Pagels et al. (2009) who measured soot particle collapse after coating with  $\text{H}_2\text{SO}_4$  with Transmission Electron Microscopy (TEM) in conjunction with DMA-APM techniques. Previous work by Kutz and Schmidt-Ott (1992) has suggested that the driving force for agglomerate rearrangement is the surface tension force of the condensed material on the soot core. The surface tension of DOS is much smaller than that of  $\text{H}_2\text{SO}_4$ . The suggested surface tension mechanism is a possible explanation for the observed difference in the  $\text{H}_2\text{SO}_4$  and DOS rearrangement.

#### 4.2. Comparison of CPMA and AMS-SMPS Instruments

Both the CPMA and AMS-SMPS instruments provide particle mass determination for size selected aerosol particles. There is however an important difference between the data provided by the two instruments. The CPMA yields the total per-particle mass and does not provide a separate evaluation of the black carbon mass in the particle. (Recall that the data shown in Figure 5 are obtained in two separate sequential runs: nascent, then denuded.) The AMS instrument directly measures the non-refractory mass of the particles (i.e., chemical components that

readily vaporize at  $600^\circ\text{C}$  and  $\sim 10^{-7}$  torr). The combination of the AMS and SMPS measurements provides a means for determining the refractory (i.e., black carbon) mass in the same particle, via a system of equations described in DeCarlo et al. (2004) and Slowik et al. (2004). The objective of this section is to inter-compare the CPMA and AMS-SMPS mass measurements.

Figure 9 plots the per-particle mass obtained via the AMS-SMPS measurements as a function of the CPMA-measured particle mass for (a) nascent soot generated at  $\phi = 5.0 \pm 0.2$ , (b) nascent soot generated at  $\phi = 2.0 \pm 0.2$ , (c) DOS-coated soot ( $\phi = 2.0 \pm 0.2$ ), and (d)  $\text{H}_2\text{SO}_4$ -coated soot ( $\phi = 2.0 \pm 0.2$ ). The AMS-SMPS mass measurements were obtained using the measured  $d_{va}$ ,  $d_m$ , and non-refractory composition of the particles as discussed in DeCarlo et al. (2004) and Slowik et al. (2004).

As was stated, the BC mass provided with the AMS-SMPS instrument is not directly measured, rather the mass is calculated via a system of equations based on the measured  $d_{va}$ ,  $d_m$  and non-refractory composition of the particles (Slowik et al. 2004). The overall uncertainty of the AMS-SMPS method for mass determination is principally governed by the uncertainty of the  $d_{va}$  and  $d_m$  measurements. For this experiment, the uncertainty

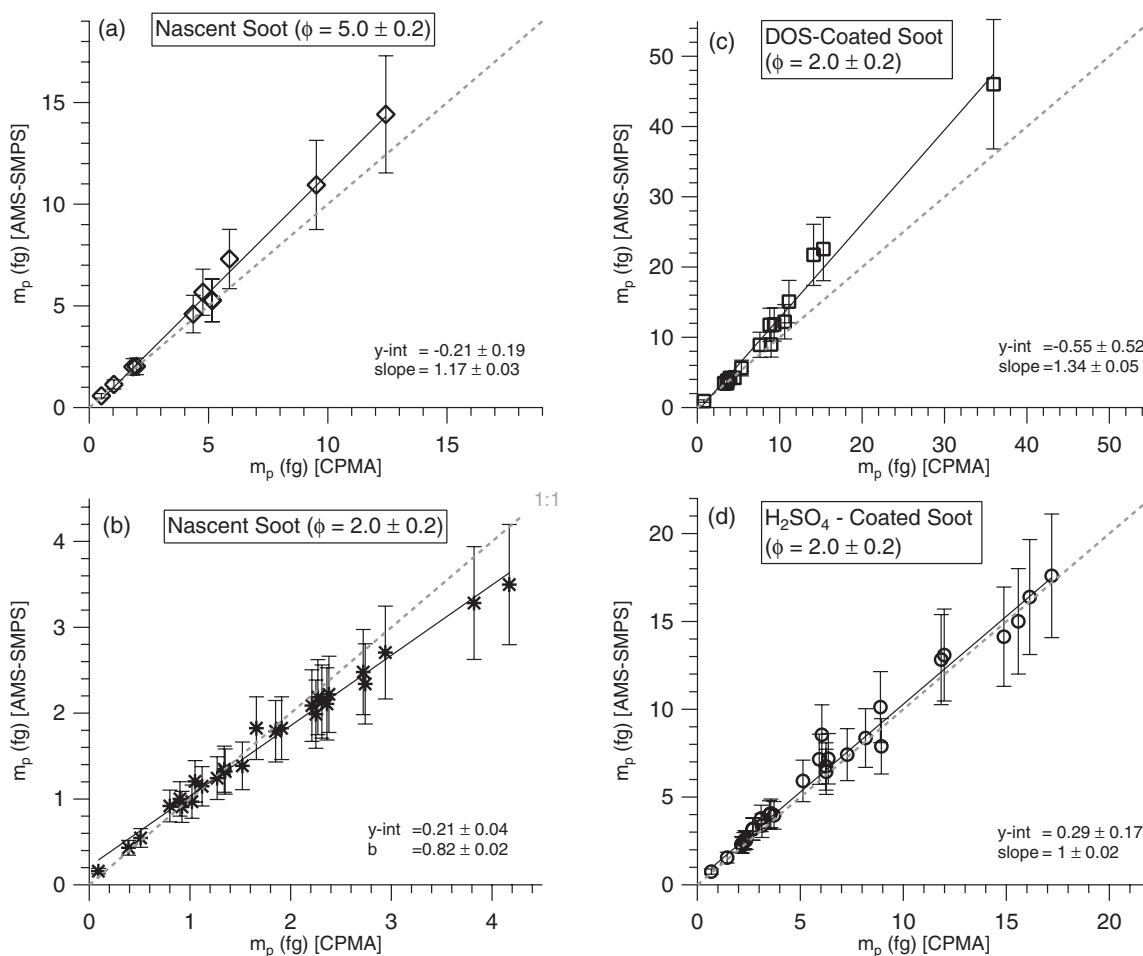


FIG. 9. Per-particle mass obtained via the AMS-SMPS measurements versus the CPMA-measured particle mass for (a) nascent soot generated at  $\phi = 5.0 \pm 0.2$ , (b) nascent soot generated at  $\phi = 2.0 \pm 0.2$ , (c) DOS-coated soot ( $\phi = 2.0 \pm 0.2$ ), and (d) H<sub>2</sub>SO<sub>4</sub>-coated soot ( $\phi = 2.0 \pm 0.2$ ). The slope and intercept of linear fits to the data are shown in each panel. The 1:1 line is shown as the dashed line in each plot. Note the different axes in each panel, a consequence of the different mass ranges obtained for each particle type studied.

in the AMS-SMPS mass is estimated to be  $\pm 20\%$ . For the H<sub>2</sub>SO<sub>4</sub>-coated soot particles, the two mass measurements are in agreement. For the heavily coated soot particles ( $\phi = 5.0 \pm 0.2$  ( $\sim 0.74$  non-refractory mass fraction) and DOS-coated ( $0.10$ – $0.99$  organic mass fraction), the SMPS-AMS measurements are  $\sim 17\%$  and  $30\%$  higher than the CPMA measurements. For the nascent soot particles produced at  $\phi = 2.0 \pm 0.2$ , the SMPS-AMS mass measurements is  $\sim 18\%$  lower than the corresponding CPMA measurements. Overall, we consider the agreement between these two independent measurements of mass to be reasonable.

### 4.3. Performance of the SP2 Instruments

Three Single Particle Soot Photometer (SP2) instruments were tested in these studies. The instruments were from the University of Hawaii (UH), Droplet Measurement Technologies (DMT), and the National Oceanic and Atmospheric Administration Chemical Sciences Division (NOAA, CSD). The

experiments with the SP2 instruments had the following goals: (a) measure, inter-compare and calibrate the incandescence signals obtained from the three SP2 instruments as a function of black carbon particle mass; (b) determine the effect of particle shape on the SP2 measurement of BC mass; (c) investigate how DOS and H<sub>2</sub>SO<sub>4</sub> coatings affect the SP2 measurement of BC mass; (d) determine the lower limit for BC mass detection in the SP2; and (e) determine SP2 response for several types of atomized carbonaceous materials – this latter aspect of instrument performance (item “e”) will be discussed in a separate publication.

#### 4.3.1. Inter-comparison and calibration of the incandescence SP2 signals

The nomenclature associated with the various forms of carbon-containing aerosol at varying levels of purity is generally vague and complex. The SP2, through its detection scheme, measures only the mass of refractory material capable of

reaching temperatures of  $\sim 4000$  K without vaporizing. We refer to the SP2 determination here, then, as being appropriate for “refractory black carbon” (rBC), as discussed in deeper detail in Schwarz et al. (2010). In the measurements of carbon-containing combustion aerosol here and in the atmosphere this material is believed to be equivalent to “black carbon” as used in measurements of optical absorption, and most refractory components of EC identified by thermal decomposition analysis.

Figure 10 displays the incandescence signal for the three SP2 instruments as a function of total per-particle mass measured by the CPMA instrument for denuded soot particles produced at  $\phi = 2.0 \pm 0.2$ . Three different types of denuded particle are displayed in the figure: (1) nascent-denuded, (2) DOS-coated and denuded, and (3)  $\text{H}_2\text{SO}_4$ -coated and denuded. Because the soot particles are denuded they are primarily composed of black carbon. Therefore, for the denuded subset of experimental runs, the CPMA-measured particle mass is also the BC mass. As can be seen in Figure 10, SP2 response is a linear function of the BC mass of the particles. The linear fit (using all denuded particle types) for each SP2 instrument provides a per-particle incandescence-to-BC mass calibration for the individual SP2 instruments.

While the absolute magnitudes of the incandescence signals for the three instruments differ due to differences in the operating conditions and settings of each SP2, each calibration curve fits a straight line correlation with  $R^2 = 0.98$ .

#### 4.3.2. Effect of particle shape on SP2 measurements

Given the different types of denuded particles displayed in Figure 10, it is possible to examine the influence of BC particle shape on the SP2 incandescence signal. Recall from Figures 7 and 8 that the  $\text{H}_2\text{SO}_4$ -coated-denuded particles undergo rearrangement resulting in a partially collapsed, more compact BC core. This is in contrast to the nascent-denuded and DOS-coated-denuded particles, which retain their fractal shape. The data in Figure 10 show no measurable difference in SP2 incandescence between the collapsed ( $\text{H}_2\text{SO}_4$ -coated-denuded) and fractal (nascent or DOS-coated-denuded) soot. This result indicates that SP2 incandescence is independent of particle shape within the range of denuded morphologies and particle sizes tested during the inter-comparison ( $2.1 < D_{fm} < 2.5$ ).

#### 4.3.3. Effect of coatings on SP2 measurements

To determine the influence of coatings (condensed organics from the flame, DOS, or  $\text{H}_2\text{SO}_4$ ) on the SP2 instrument response we plot in Figure 11 the SP2-measured incandescent mass for coated soot particles as a function of the SP2-measured incandescent mass for the corresponding denuded particles (with the coating material removed). Data shown in the figure were obtained with the NOAA SP2 instrument. Similar results were obtained with the UH and DMT SP2 instruments. The format of Figure 11 is similar to Figure 5 that presented the CPMA-measured mass for correlated nascent and denuded soot runs.

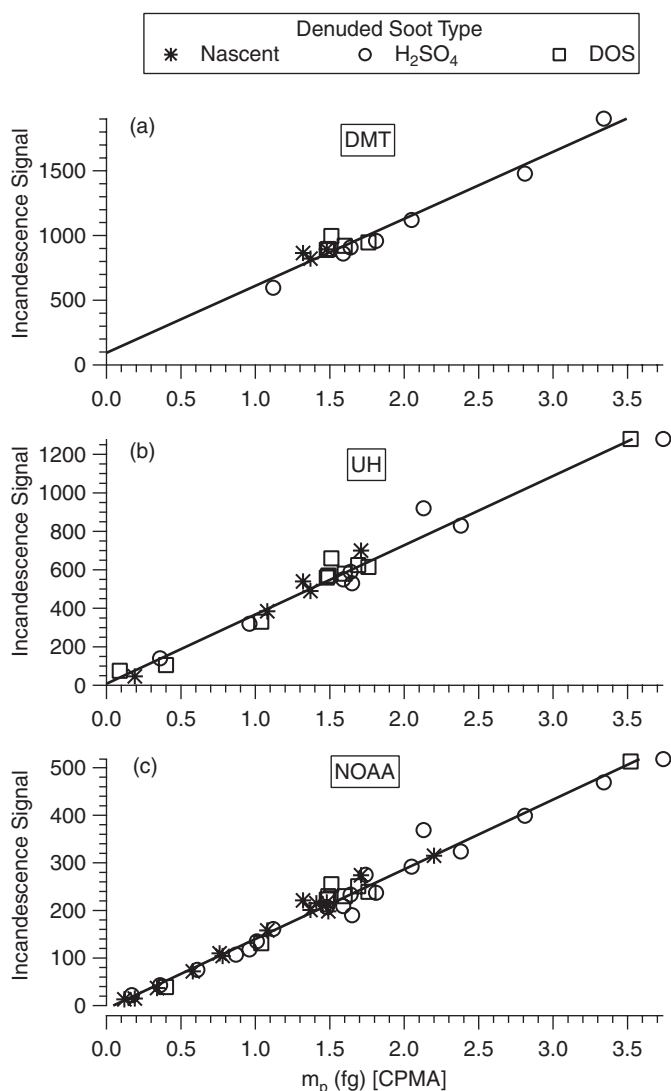


FIG. 10. Incandescence signal for the three SP2 instruments plotted versus the CPMA-measured mass. Experiments were performed with denuded soot particles produced at  $\phi = 2.0 \pm 0.2$ . Three different denuded particle types are shown: (1) nascent-denuded (stars) (2) DOS-coated-denuded (open squares), and (3)  $\text{H}_2\text{SO}_4$ -coated-denuded (open circles). Denuded soot particles are primarily composed of black carbon. Therefore, the CPMA-measured particle mass is also the BC mass and each plot provides an empirical incandescence mass calibration for the specific SP2 instrument. The  $R^2$  value for the linear fits is 0.98 for all three instruments. Linear fits are based on the instrument response to all three denuded particle types. The different slopes between the three instruments merely represent three choices of operational gain for the detectors.

Here, the SP2 measurement of BC can be directly compared in the presence and absence of substantial amounts of non-absorbing coatings.

A linear fit through the data points in Figure 11 (solid line) has a slope of 0.99 and  $R^2 = 0.99$ . This result indicates that across the range of coating types and thicknesses studied during the inter-comparison the SP2 determination of black carbon mass remained accurate. These observations are

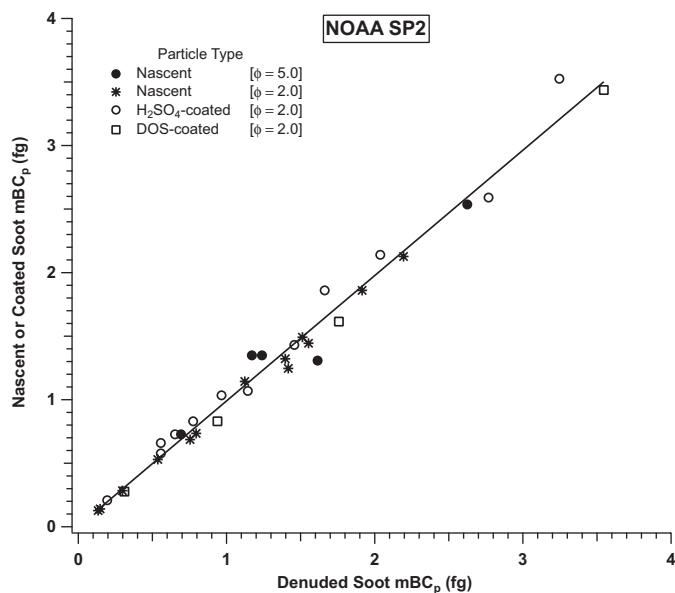


FIG. 11. SP2-measured BC mass ( $mBC_p$ ) for coated soot particles: nascent  $\phi = 5.0 \pm 0.2$ , nascent  $\phi = 2.0 \pm 0.2$ , DOS-coated  $\phi = 2.0 \pm 0.2$ , and  $H_2SO_4$ -coated  $\phi = 2.0 \pm 0.2$  plotted as a function of the SP2-measured  $mBC_p$  for the corresponding denuded soot particles. Slope of a linear fit to the data (shown as the solid line) is  $0.99 \pm 0.02$  with a  $R^2 = 0.99$ .

consistent with the results obtained for oleic acid and anthracene coatings in the first inter-comparison study (Slowik et al. 2007a).

#### 4.3.4. Lower detection limit for measurement of BC mass in soot particles

One of the objectives of the inter-comparison study was to determine the detection limit of the SP2 instrument when operated under typical SP2 laser intensity settings. The specifics of such determinations are discussed in Schwarz et al. (2010). Here we simply note that, based on the results from the inter-comparison project, the SP2 instrument (under typical operating conditions) can reliably measure absorbing particles with volume-equivalent diameter ( $d_{ve}$ )  $\geq 90$  nm (BC mass of  $\sim 0.7$  fg).

## 5. EXPERIMENTAL OBJECTIVES AND SELECTED RESULTS FOR OPTICAL ABSORPTION, SCATTERING AND EXTINCTION BASED INSTRUMENTS

As listed in Table 1b, the present inter-comparison study included instruments that measure optical absorption, scattering, and extinction. The following real-time absorption instruments were tested: NOAA Photoacoustic Spectrometer (PAS), Photo-Acoustic Soot Spectrometer (PASS-3), and Photo-Thermal Interferometer (PTI). The NOAA PAS and PTI instruments measure absorption at  $\lambda = 532$  nm. The PASS-3 measures absorption and scattering at  $\lambda = 405$  nm, 532 nm, and 781 nm.

The real-time extinction instruments tested were the NOAA Cavity Ring Down Aerosol Extinction Spectrometer (CRD-

AES) and Cavity Attenuated Phase Shift Extinction Monitor (CAPS). The CRD-AES instrument operates at three wavelengths,  $\lambda = 355$  nm,  $\lambda = 532$  nm, and  $\lambda = 1064$  nm. The CAPS instrument operates at  $\lambda = 445$  nm.

The goals for the optically-based instrumentation were to: (a) combine the optical and mass-based measurements to obtain the mass specific absorption coefficient ( $MAC$ ) for denuded soot particles; (b) determine the effect, if any, of particle shape on absorption and extinction measurements; (c) determine the  $\lambda$ -dependence of the  $\sigma_{abs}$  and  $\sigma_{ext}$ ; (d) determine the effect of non-absorbing coatings (condensed organics from the flame, DOS, or  $H_2SO_4$ ) on  $\sigma_{abs}$ ; and (e) track changes in the single scattering albedo ( $SSA$ ) of coated soot particles.

### 5.1. Performance Study of the PAS, PASS-3 and PTI Instruments

#### 5.1.1. Mass Specific Absorption Coefficient for Denuded Soot Particles

The mass specific absorption coefficient ( $MAC$ ) is related to the absorption cross-section and particle mass as shown in Equation (3):

$$\sigma_{abs} = MAC \cdot m_p \quad [3]$$

The absorption cross-section is typically expressed in units of  $m^2$ /particle and the mass specific absorption coefficient in units of  $m^2/g$ . Therefore, simultaneous measurements of aerosol absorption, particle number concentration and particle mass provide the parameters necessary for  $MAC$  determination.

Figure 12 displays  $\sigma_{abs}$  at  $\lambda = 532$  nm for denuded soot measured with the PASS-3, PTI, and PAS as a function of the mass determined with the CPMA instrument. (Note that  $\sigma_{abs}$  is calculated from ensemble absorption normalized to the particle number concentration.) Three types of denuded particles are shown in the figure: DOS-coated-denuded (green squares),  $H_2SO_4$ -coated-denuded (red circles), and nascent-denuded (black stars). All data shown in Figure 12 are for soot cores generated at  $\phi = 2.0 \pm 0.2$  with q1 number fractions  $\geq 0.93$ . Prior to denuding, the DOS and  $H_2SO_4$  coating mass fractions ranged from 0.4–0.99.

The  $\sigma_{abs}$  values together with the CPMA mass measurement yields  $MAC$  values =  $8.11 \pm 1.7$   $m^2/g$ ,  $7.43 \pm 0.5$   $m^2/g$ , and  $8.68 \pm 0.4$   $m^2/g$  for the PASS-3, PTI, and PAS respectively. Within experimental accuracy ( $1\sigma$  standard deviation), the  $MAC$  values obtained with the PASS-3 and PAS instruments are in agreement ( $8.11 \pm 1.7$   $m^2/g$  and  $8.68 \pm 0.4$   $m^2/g$  respectively). The  $MAC$  value provided by the PTI instrument is slightly lower ( $7.43 \pm 0.5$   $m^2/g$ ) than the  $MAC$  values obtained with the PASS-3 and PAS instruments. The  $MAC$  values obtained here for denuded flame-generated soot particles can be compared to  $MAC = 7.5 \pm 1.2$   $m^2/g$  (at  $\lambda = 530$  nm) measured for laboratory-generated kerosene soot (Sheridan et al. 2005), and a value of  $MAC = 7.5 \pm 1.2$   $m^2/g$  (at  $\lambda = 550$  nm) for light absorbing

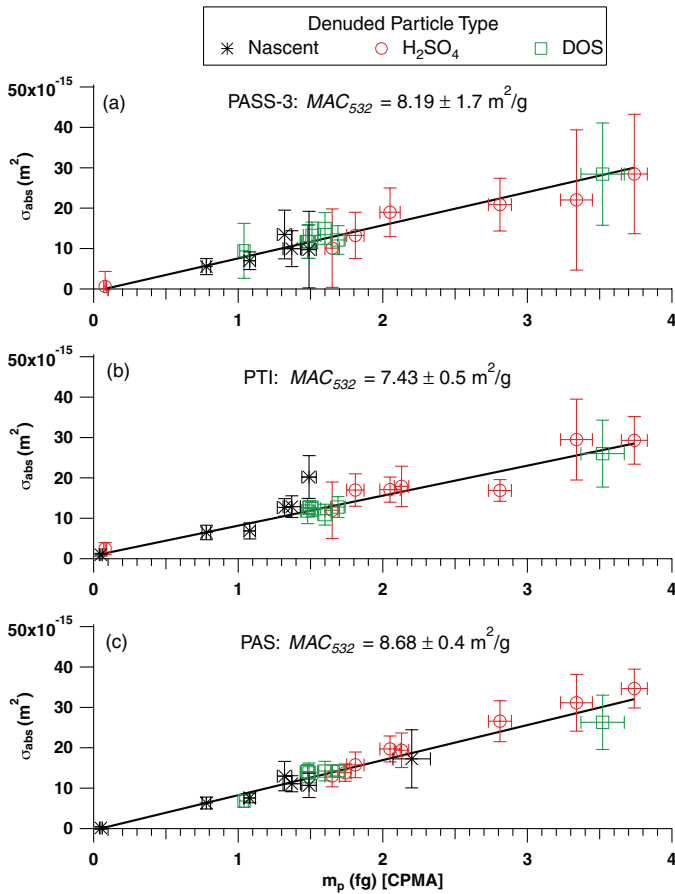


FIG. 12. Absorption cross-sections ( $\sigma_{abs}$ ) for denuded soot measured at  $\lambda = 532$  nm for the (a) PASS-3, (b) PTI, and (c) PAS instruments as a function of the mass measured by the CPMA instrument. Soot particles were generated at  $\phi = 2.0 \pm 0.2$ . The symbols indicate the different coating condition (prior to denuding): DOS-coated-denuded (green squares),  $\text{H}_2\text{SO}_4$ -coated-denuded (red circles) or nascent-denuded (black stars). The linear regressions shown are fit through all three denuded particle types (weighted to the  $1\sigma$  standard deviations shown). The slope of each linear fit is the mass specific absorption coefficient ( $MAC$ ).

aerosol measured at or near the source. (Compiled from multiple studies in a review by Bond and Bergstrom 2006a.) In addition, these results suggest that there is no difference in  $\sigma_{abs}$  resulting from the partial collapse of the fractal soot observed for the  $\text{H}_2\text{SO}_4$ -coated-denuded runs. If this were the case, then the  $\sigma_{abs}$  for the  $\text{H}_2\text{SO}_4$ -coated-denuded trials should fall off the line determined by the nascent-denuded and DOS-coated-denuded trials. Unfortunately, few of the  $\text{H}_2\text{SO}_4$  points actually overlap with the nascent or DOS points, which would help to strengthen this conclusion. This will be a focus of future studies.

## 5.2. Wavelength Dependence of $\sigma_{abs}$ and $\sigma_{ext}$ for Denuded Soot Particles

In addition to  $\lambda = 532$  nm, the PASS-3 also measures absorption at  $\lambda = 405$  nm and  $\lambda = 781$  nm. The additional wavelength information is shown in Figure 13 which displays absorption

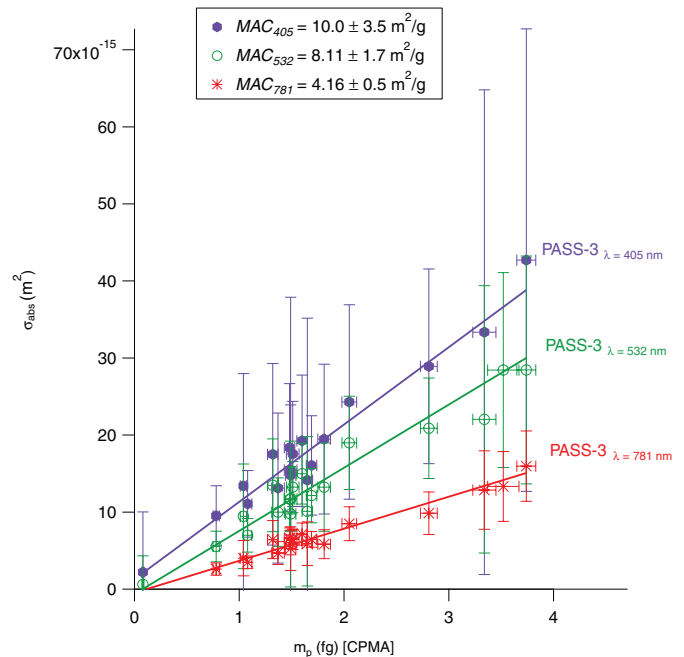


FIG. 13. Absorption cross-sections ( $\sigma_{abs}$ ) for the PASS-3 at  $\lambda = 405$  nm, 532 nm, and 781 nm as a function of CPMA-measured mass for denuded soot particles generated at  $\phi = 2.0 \pm 0.2$  (including nascent-denuded, DOS-coated-denuded and  $\text{H}_2\text{SO}_4$ -coated-denuded). The slope of each line is the mass specific absorption coefficient ( $MAC$ ) for the corresponding wavelength.

cross-sections for  $\lambda = 405$  nm,  $\lambda = 532$  nm (repeated from Figure 12), and  $\lambda = 781$  nm as a function of the mass measured with the CPMA for denuded soot.

The  $MAC$  values are obtained from linear fits to the data (weighted by  $1\sigma$  standard deviations shown). The PASS-3 yield  $MAC$  values of  $10.0 \pm 3.5$   $\text{m}^2/\text{g}$ ,  $8.11 \pm 1.7$   $\text{m}^2/\text{g}$ , and  $4.16 \pm 0.5$   $\text{m}^2/\text{g}$  for the  $\lambda = 405$  nm,  $\lambda = 532$  nm, and  $\lambda = 781$  nm respectively. As shown in the figure, the standard deviations at  $\lambda = 405$  nm are significantly higher than at  $\lambda = 532$  nm or  $\lambda = 781$  nm. The difference in the signal to noise ratios is primarily due to the different laser powers utilized in the PASS-3:  $\sim 90$  mW at  $\lambda = 405$  nm,  $\sim 200$  mW at  $\lambda = 532$  nm, and  $\sim 500$  mW at 781 nm.

While  $\sigma_{abs}$  is approximately linearly proportional to particle mass (for aerosol particles with a constant refractive index),  $\sigma_{ext}$  (which is the sum of the absorption and scattering cross-sections) will vary more strongly with particle mass (and size). This is due to increased scattering as a function of particle size. Therefore, unlike the  $MAC$  values obtained in Figure 13, the relationship between  $\sigma_{ext}$  and  $m_p$  cannot be characterized with a single mass specific extinction coefficient. However, in the domain where scattering is small (low mass, small size, longer wavelength), the absorption will dominate total extinction and as a result  $\sigma_{abs} \sim \sigma_{ext}$ .

Two instruments used in the inter-comparison study directly measure extinction: the Cavity Ring Down Aerosol Extinction

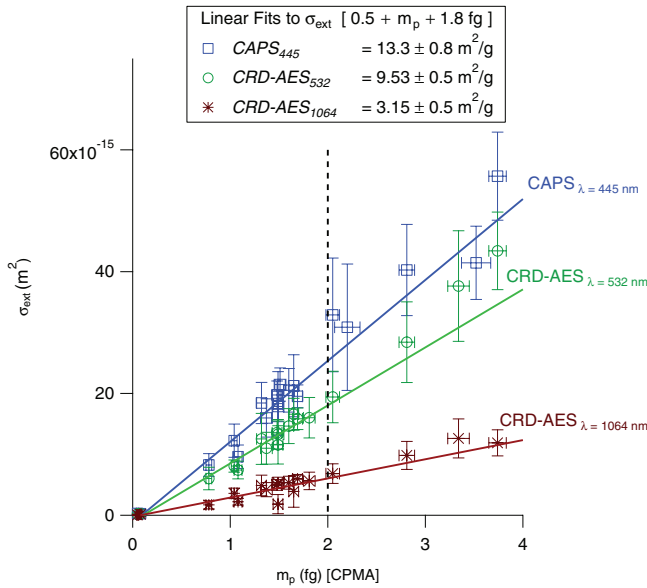


FIG. 14. Extinction cross-sections ( $\sigma_{ext}$ ) for the CRD-AES instrument at  $\lambda = 532$  nm, and  $\lambda = 1064$  nm and for the CAPS instrument at  $\lambda = 445$  nm as a function of CPMA-measured mass for denuded soot particles generated at  $\phi = 2.0 \pm 0.2$  (including nascent-denuded, DOS-coated-denuded and  $H_2SO_4$ -coated-denuded). The error bars shown are the  $1\sigma$  standard deviation.

Spectrometer (CRD-AES) and the Cavity Attenuated Phase Shift Extinction Monitor (CAPS). The CRD-AES instrument measures extinction at  $\lambda = 355$  nm,  $\lambda = 532$  nm, and  $\lambda = 1064$  nm and the CAPS measures extinction at  $\lambda = 445$  nm. Figure 14 displays  $\sigma_{ext}$  for denuded soot particles as a function of CPMA-measured particle mass. The CRD-AES data obtained at  $\lambda = 355$  nm data are excluded from the figure due to a malfunction with the 355 nm photomultiplier.

The solid lines shown in the figures are the linear fits to the low mass range data from  $0.5 \leq m_p \leq 1.8$  fg. The vertical dashed line indicates the mass below which data points were fit to the line. The slopes of the linear fits are  $13.3 \pm 0.8$  m<sup>2</sup>/g,  $9.53 \pm 0.5$  m<sup>2</sup>/g, and  $3.15 \pm 0.5$  m<sup>2</sup>/g for  $\lambda = 445$  nm,  $\lambda = 532$  nm, and  $\lambda = 1064$  nm respectively. As expected, the data in Figure 14 show increasing  $\sigma_{ext}$  with increasing particle mass and higher  $\sigma_{ext}$  at lower wavelengths. The deviation of the data points away from the straight lines shown in Figure 14 is attributed to increased scattering. As stated earlier, for denuded soot particles in the low mass range,  $\sigma_{abs} \sim \sigma_{ext}$ . For the  $\sigma_{ext}$  data obtained with the CRD-AES system at  $\lambda = 532$  nm the slope of the line shown in Figure 14 ( $9.53 \pm 0.5$  m<sup>2</sup>/g) can be compared with the MAC value of  $8.68 \pm 0.4$  m<sup>2</sup>/g obtained with the  $\lambda = 532$  nm PAS measurements for denuded soot. (The CRD-AES and PAS measurements were made in series during

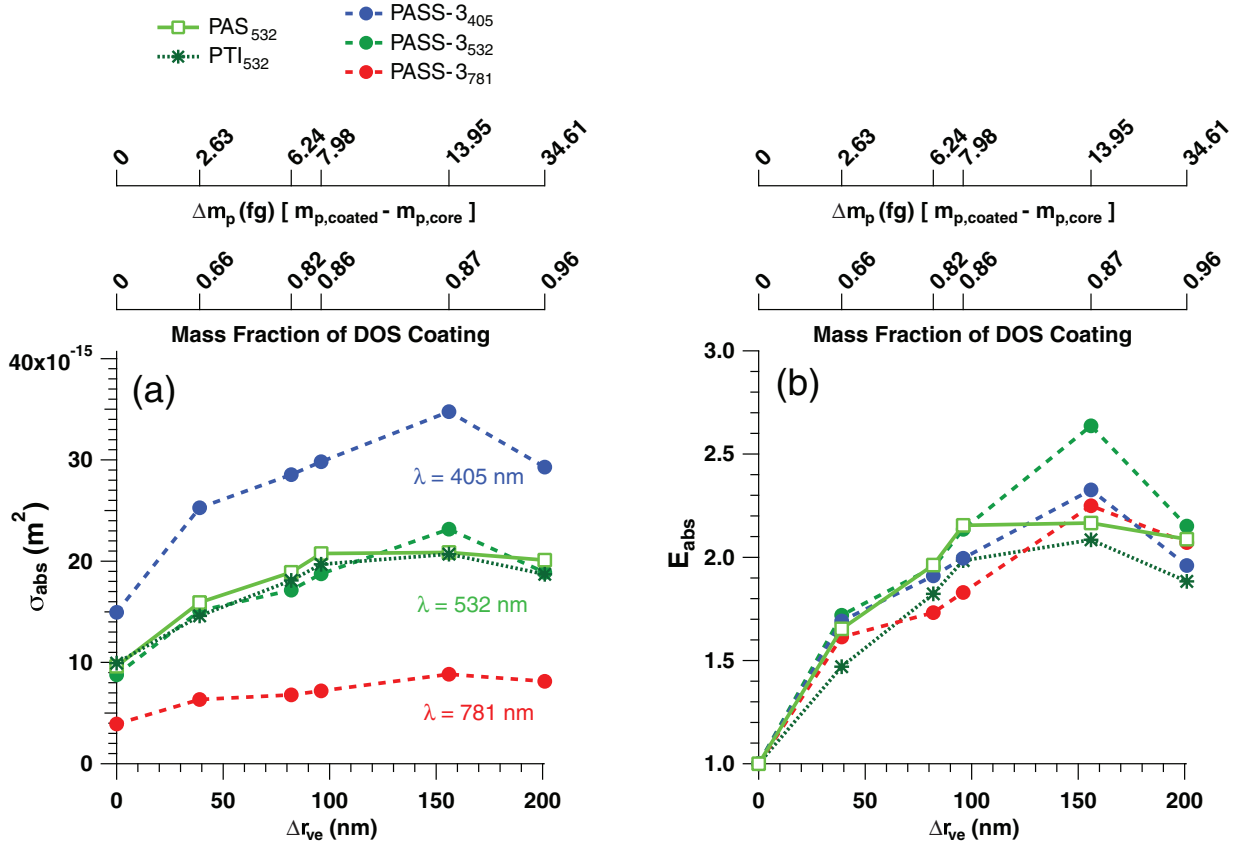


FIG. 15. (a) Measured absorption cross sections for PASS-781, PASS-532, PASS-405, PTI-532, and PAS-532 instruments for a  $d_m = 168$  nm fractal soot core coated with DOS. (b) Ratio of  $\sigma_{abs}$  for the coated particle to  $\sigma_{abs}$  of the core particle corresponding to the data in Figure 16a identified by color.

the inter-comparison study.) The slightly higher value obtained with the extinction data suggests that, even within the low mass range, denuded soot particles scatter a small amount of light in addition to their absorption.

### 5.3. Changes in Absorption and Scattering due to Non-absorbing Coatings on Soot Particles

Non-absorbing coatings have been reported to enhance the absorption cross-section of BC-containing aerosol particles based on ambient (Schwarz et al. 2008; Shiraiwa et al. 2008) and laboratory measurements (Schnaiter et al. 2005; Bond et al. 2006b; Slowik et al. 2007a; Zhang et al. 2008; Khalizov et al. 2009; Lack et al. 2009). The enhancement is likely due to lensing effects of the non-absorbing coating that concentrates the light onto the absorbing core. In Figures 15a and b we show absorption data for a fractal soot core ( $d_m = 168$  nm) produced at  $\phi = 2.0 \pm 0.2$  as a function of DOS coating thickness. The primary x-axis in each figure is the change in the volume equivalent radius ( $\Delta r_{ve}$ ) of the particles. The  $\Delta r_{ve}$  values are calculated from the volume equivalent diameter  $d_{ve}/2$  for coated and uncoated soot particles obtained from AMS and SMPS measurements, described in detail in Slowik et al. (2007b). Two additional axes along the top of each graph denote the change in the particle mass (measured with the CPMA) due to DOS coating and the DOS mass fraction. Figure 15a displays the  $\sigma_{abs}$  for the PTI, PAS, and PASS-3 instruments. Figure 15b displays the absorption enhancement ( $E_{abs} = \sigma_{abs,coated} / \sigma_{abs,core}$ ) and shows that  $E_{abs}$  increases with increasing DOS coating thickness reaching an enhancement peak of  $\sim 2$ – $2.25$  at a DOS coating thickness of  $\Delta r_{ve} \sim 100$  nm and DOS mass fraction of  $\sim 0.8$  followed by a decrease in absorption for the thickest coating ( $\Delta r_{ve} \sim 200$  nm). A possible explanation for the observed decrease in absorption enhancement at the thickest coating is the increased scattering by the heavily coated particle partially shielding the absorbing core from the incident light.

A full range of coating experiments were completed during the inter-comparison including fractal soot cores ranging from  $d_m = 50$  nm to  $d_m = 209$  nm. Each core was systematically coated with DOS or  $H_2SO_4$ . In all cases studied, an absorption enhancement of  $\sim 2$  was observed, in line with recent results from Shiraiwa et al. (2010). A detailed presentation of these results including a comparison with Mie theory core-shell calculations will be provided in a subsequent publication.

To demonstrate the effect of non-absorbing coatings on the SSA of soot particles, Figure 16 shows the change in SSA for the same  $d_m = 168$  nm fractal soot core coated with DOS shown in Figure 15. As in Figure 15, the SSA is plotted here as a function of DOS coating thickness ( $\Delta r_{ve}$ ) with additional axes along the top of each graph denoting the change in the particle mass (measured with the CPMA) and mass fraction of the DOS coating.

Two SSA curves are shown in Figure 16. One is obtained through the combination of the CRD-AES extinction and PAS absorption data at  $\lambda = 532$  nm and the other is obtained with

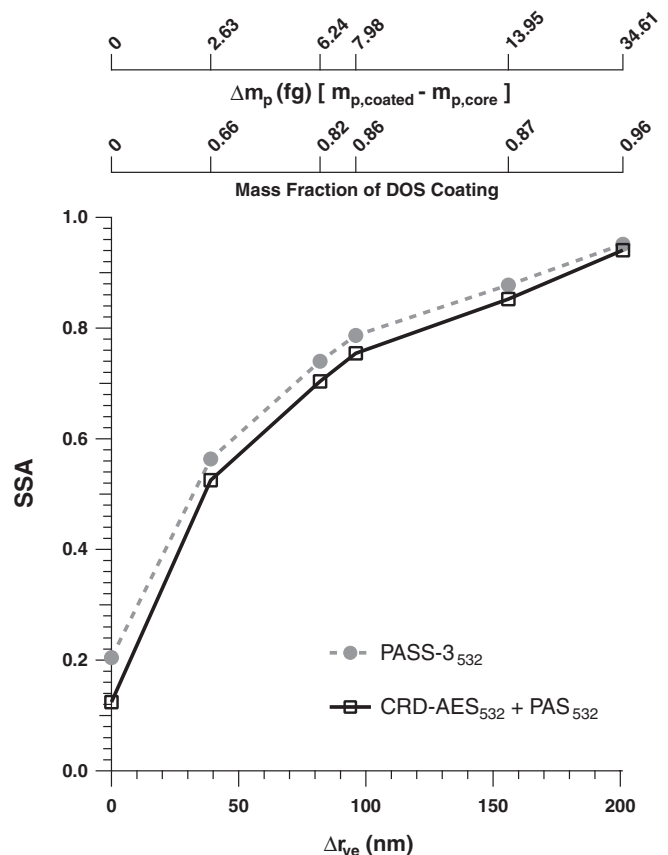


FIG. 16. Single scattering albedo (SSA) calculated from the combined CRD-AES/PAS 532 nm data, and the 532 nm PASS-3 data for  $d_m = 168$  nm fractal soot core coated with multiple thicknesses of DOS.

the  $\lambda = 532$  nm absorption and scattering measurements of the PASS-3 instrument. The change in SSA obtained with the PASS-3 instrument is in good agreement with the SSA measured with the CRD-AES – PAS instrument combination. The SSA is shown to increase from an initial value of  $\sim 0.12$ – $0.20$  for the nascent  $d_m = 168$  nm soot core to  $\sim 0.94$  for heaviest DOS-coating (DOS mass fraction of 0.96,  $\Delta r_{ve} = 201$  nm). In comparison to the laboratory SSA values shown here, ambient SSA, determined from scattering and extinction measurements, were reported to vary between 0.60 and 0.85 from early morning to mid-day (Paredes-Miranda et al. 2009).

## 6. SUMMARY

An inter-comparison study of instruments designed to measure black carbon particle properties was completed. Eighteen instruments were tested, including 7 mass-based (CPMA, AMS-SMPS, SP-AMS, SP2 (3 in number), PAS2000CE), and 9 optically based (PAS, PTI, PASS-3, CRD-AES, CAPS, MAAP, PSAP (2 in number), Nephelometer) as well as 2 filter samples for OCEC and SEM analyses. The study covered an experimental matrix of 318 runs that systematically tested the

performance of each instrument across a range of parameters including: fuel equivalence ratio ( $1.8 \leq \phi \leq 5$ ) particle mobility size ( $30 \leq d_m \leq 300$  nm), mass-mobility exponent ( $2.0 \leq D_{fm} \leq 3.0$ ), black carbon mass ( $0.07 \leq m_{BC} \leq 4.2$  fg) and particle chemistry and density (changed via coatings). In coated runs, particles were coated with sulfuric acid or dioctyl sebacate (DOS) ( $0.5 \leq \Delta r_{ve} \leq 201$  nm).

Mass measurements provided by the CPMA were validated with PSL particles of known size and density. Coupled CPMA mass measurements for nascent and then denuded soot particles generated at  $\phi = 2.0$  and  $\phi = 5.0$  provided the black carbon mass in soot produced at different equivalence ratios. Combined CPMA-DMA measurements of  $m_p$  and  $d_m$  were used to determine the mass-mobility exponent of nascent soot, coated soot, and denuded soot particles. Results indicate that DOS-coated-denuded fractal soot particles substantially retain their fractal aggregate morphology ( $D_{fm} = 2.17$ ) while H<sub>2</sub>SO<sub>4</sub>-coated-denuded fractal soot particles undergo rearrangement of the fractal core to a more compact morphology ( $D_{fm} = 2.49$ ). Total particle mass measurements with the AMS-SMPS technique compared well with CPMA measurements across the range of particle compositions studied.

Incandescence signals from the three SP2 instruments were calibrated with respect to the CPMA-measured mass for denuded soot particles. Incandescence was found to be independent of particle shape and the type and thickness of non-absorbing coatings studied.

Absorption measurements at  $\lambda = 532$  with the PASS-3, PTI, and PAS instruments combined with the CPMA mass measurement provided mass specific absorption coefficients (MAC) for denuded soot particles of  $8.11 \pm 1.7$  m<sup>2</sup>/g,  $7.43 \pm 0.5$  m<sup>2</sup>/g,  $8.68 \pm 0.4$  m<sup>2</sup>/g, respectively. Additional MAC values of  $10.0 \pm 3.5$  m<sup>2</sup>/g and  $4.16 \pm 0.5$  m<sup>2</sup>/g were obtained for denuded soot measured at the  $\lambda = 405$  nm and  $\lambda = 781$  nm with the PASS-3 instrument.

Extinction measurements with the CAPS ( $\lambda = 445$  nm) and CRD-AES ( $\lambda = 532$  nm and  $\lambda = 1064$  nm) combined with the CPMA mass measurement were used to examine the change in extinction cross-section as a function of mass for denuded soot particles.

Absorption enhancement was observed for a fractal soot core ( $d_m = 168$  nm) coated with DOS. The enhancement reached a plateau of  $\sim 2$  for DOS coating thickness of  $\Delta r_{ve} \sim 100$  nm and DOS mass fraction  $> 0.8$ . The CRD-AES/PAS and PASS-3 instruments were used to measure the single scattering albedo of the DOS-coated  $d_m = 168$  nm fractal soot core. As the thickness of the DOS coating increased the SSA continuously increased, from  $\sim 0.12$  for the nascent soot particles to  $\sim 0.94$  for the thickest DOS coating ( $\Delta r_{ve} \sim 201$  nm).

## REFERENCES

Abu-Rahmah, A., Arnott, W. P., and Moosmuller, H. (2006). Integrating Nephelometer with a Low Truncation Angle and an Extended Calibration Scheme. *Measurement Sci. & Technol.* 17:1723–1732.

- Allan, J. D., Jimenez, J. L., Williams, P. I., Alfarra, M. R., Bower, K. N., Jayne, J. T., Coe, H., and Worsnop, D. R. (2003). Quantitative Sampling using an Aerodyne Aerosol Mass Spectrometer – I. Techniques of Data Interpretation and Error Analysis. *J. Geophys. Res.–Atmospheres* 108: NO. D3, 4090, doi:10.1029/2002JD002358
- Atkinson, D. B. (2003). Solving Chemical Problems of Environmental Importance using Cavity Ring-Down Spectroscopy. *Analyst* 128:117–125.
- Baynard, T., Lovejoy, E. R., Pettersson, A., Brown, S. S., Lack, D., Osthoff, H., Massoli, P., Bond, T. C., Anderson, T. L., and Campbell, D. (1999). Calibration and Intercomparison of Filter-Based Measurements of Visible Light Absorption by Aerosols. *Aerosol Sci. Technol.* 30:582–600.
- Bond, T. C., and Bergstrom, R. W. (2006a). Light Absorption by Carbonaceous Particles: An Investigative Review. *Aerosol Sci. Technol.* 40:27–67.
- Bond, T. C., Habib, G., and Bergstrom, R. W. (2006b). Limitations in the Enhancement of Visible Light Absorption Due to Mixing State. *J. Geophys. Res.–Atmospheres* 111.
- Bulatov, V., Fisher, M., and Schechter, I. (2002). Aerosol Analysis by Cavity-Ring-Down Laser Spectroscopy. *Analytica Chimica Acta* 466:1–9.
- Campillo, A. J., and Lin, H. B. (1981). Photothermal Spectroscopy of Aerosols. *Proc. the Society of Photo-Optical Instrumentation Engineers* 286: 24–32.
- Canagaratna, M. R., Jayne, J. T., Ghertner, D. A., Herndon, S., Shi, Q., Jimenez, J. L., Silva, P. J., Williams, P., Lanni, T., Drewnick, F., Demerjian, K. L., Kolb, C. E., and Worsnop, D. R. (2004). Chase Studies of Particulate Emissions from in-use New York City Vehicles. *Aerosol Sci. Technol.* 38:555–573.
- Canagaratna, M. R., Jayne, J. T., Jimenez, J. L., Allan, J. D., Alfarra, M. R., Zhang, Q., Onasch, T. B., Drewnick, F., Coe, H., Middlebrook, A., Delia, A., Williams, L. R., Trimborn, A. M., Northway, M. J., DeCarlo, P. F., Kolb, C. E., Davidovits, P., and Worsnop, D. R. (2007). Chemical and Microphysical Characterization of Ambient Aerosols with the Aerodyne Aerosol Mass Spectrometer. *Mass Spectrometry Reviews* 26:185–222.
- Chakrabarty, R. K., Moosmuller, H., Arnott, W. P., Garro, M. A., Tian, G. X., Slowik, J. G., Cross, E. S., Han, J. H., Davidovits, P., Onasch, T. B., and Worsnop, D. R. (2009). Low Fractal Dimension Cluster-Dilute Soot Aggregates from a Premixed Flame. *Physical Review Letters* 102:1–4.
- Chakrabarty, R. K., Moosmuller, H., Garro, M. A., Arnott, W. P., Walker, J., Susott, R. A., Babbitt, R. E., Wold, C. E., Lincoln, E. N., and Hao, W. M. (2006). Emissions from the Laboratory Combustion of Wildland Fuels: Particle Morphology and Size. *J. Geophys. Res.–Atmospheres* 111: D07204, doi:10.1029/2005JD006659
- Cross, E. S., Onasch, T. B., Canagaratna, M., Jayne, J. T., Kimmel, J., Yu, X. Y., Alexander, M. L., Worsnop, D. R., and Davidovits, P. (2009). Single Particle Characterization using a Light Scattering Module Coupled to a Time-of-Flight Aerosol Mass Spectrometer. *Atmos. Chem. Phys.* 9:7769–7793.
- Cross, E. S., Slowik, J. G., Davidovits, P., Allan, J. D., Worsnop, D. R., Jayne, J. T., Lewis, D. K., Canagaratna, M., and Onasch, T. B. (2007). Laboratory and Ambient Particle Density Determinations using Light Scattering in Conjunction with Aerosol Mass Spectrometry. *Aerosol Sci. Technol.* 41:343–359.
- Curtius, J., Sierau, B., Arnold, F., Baumann, R., Busen, R., Schulte, P., and Schumann, U. (1998). First Direct Sulfuric Acid Detection in the Exhaust Plume of a Jet Aircraft in Flight. *Geophys. Res. Letters* 25: NO. D6, 923–926.
- Davis, C. C. (1980). Trace Detection in Gases using Phase Fluctuation Optical Heterodyne Spectroscopy. *Applied Physics Letters* 36:515–518.
- DeCarlo, P. F., Slowik, J. G., Worsnop, D. R., Davidovits, P., and Jimenez, J. L. (2004). Particle Morphology and Density Characterization by Combined Mobility and Aerodynamic Diameter Measurements. Part I: Theory. *Aerosol Sci. Technol.* 38:1185–1205.
- Fluckiger, D. U., Lin, H. B., and Marlow, W. H. (1985). Composition Measurement of Aerosols of Submicrometer Particles by Phase Fluctuation Absorption-Spectroscopy. *Applied Optics* 24:1668–1681.
- Grieshop, A. P., Reynolds, C. C. O., Kandlikar, M., and Dowlatabadi, H. (2009). A Black-Carbon Mitigation Wedge. *Nature Geo. Sci.* 2:533–534.

- Hansen, A. D. A., Rosen, H., and Novakov, T. (1984). The Aethalometer – an Instrument for the Real-Time Measurement of Optical-Absorption by Aerosol Particles. *Sci. Total Environ.* 36:191–196.
- Heintzenberg, J., and Charlson, R. J. (1996). Design and Applications of the Integrating Nephelometer: A Review. *J. Atmos. Oceanic Technol.* 13:987–1000.
- Huffman, J. A., Ziemann, P. J., Jayne, J. T., Worsnop, D. R., and Jimenez, J. L. (2008). Development and Characterization of a Fast-Stepping/Scanning Thermodeuder for Chemically-Resolved Aerosol Volatility Measurements. *Aerosol Sci. Technol.* 42:395–407.
- Jacobson, M. Z. (2001). Strong Radiative Heating due to the Mixing State of Black Carbon in Atmospheric Aerosols. *Nature* 409:695–697.
- Jayne, J. T., Leard, D. C., Zhang, X. F., Davidovits, P., Smith, K. A., Kolb, C. E., and Worsnop, D. R. (2000). Development of an Aerosol Mass Spectrometer for Size and Composition Analysis of Submicron Particles. *Aerosol Sci. Technol.* 33:49–70.
- Jiang, M., Marr, L. C., Dunlea, E. J., Herndon, S. C., Jayne, J. T., Kolb, C. E., Knighton, W. B., Rogers, T. M., Zavala, M., Molina, L. T., and Molina, M. J. (2005). Vehicle Fleet Emissions of Black Carbon, Polycyclic Aromatic Hydrocarbons, and other Pollutants Measured by a Mobile Laboratory in Mexico City. *Atmos. Chem. Phys.* 5:3377–3387.
- Jimenez, J. L., Jayne, J. T., Shi, Q., Kolb, C. E., Worsnop, D. R., Yourshaw, I., Seinfeld, J. H., Flagan, R. C., Zhang, X. F., Smith, K. A., Morris, J. W., and Davidovits, P. (2003). Ambient Aerosol Sampling using the Aerodyne Aerosol Mass Spectrometer. *J. Geophys. Res.—Atmospheres* 108: NO. D7, 8425, doi:10.1029/2001JD001213
- Kebabian, P. L., Robinson, W. A., and Freedman, A. (2007). Optical Extinction Monitor Using CW Cavity Enhanced Detection. *Review of Scientific Instruments* 78, 063102, doi:10.1063/1.2744223
- Khalizov, A. F., Xue, H. X., Wang, L., Zheng, J., and Zhang, R. Y. (2009). Enhanced Light Absorption and Scattering by Carbon Soot Aerosol Internally Mixed with Sulfuric Acid. *J. Physical Chemistry A* 113:1066–1074.
- Kim, S. C., Wang, J., Emery, M. S., Shin, W. G., Mulholland, G. W., and Pui, D. Y. H. Structural Property Effect of Nanoparticle Agglomerates on Particle Penetration through Fibrous Filter. *Aerosol Sci. Technol.* 43: 344–355.
- Kittelson, D. B. (1998). Engines and Nanoparticles: A Review. *J. Aerosol Sci.* 29:575–588.
- Kutz, S., and Schmidt-Ott, A. (1992). Characterization of Agglomerates by Condensation-Induced Restructuring. *J. Aerosol Sci.* 23:S357–S360.
- Kuwata, M., Kondo, Y., and Takegawa, N. (2009). Critical Condensed Mass for Activation of Black Carbon as Cloud Condensation Nuclei in Tokyo. *J. Geophys. Res.—Atmospheres* 114: D20202, doi:10.1029/2009JD012086
- Lack, D. A., Cappa, C. D., Cross, E. S., Massoli, P., Ahern, A. T., Davidovits, P., and Onasch, T. B. (2009). Absorption Enhancement of Coated Absorbing Aerosols: Validation of the Photo-Acoustic Technique for Measuring the Enhancement. *Aerosol Sci. Technol.* 43:1006–1012.
- Marr, L. C., Grogan, L. A., Wohrnschimmel, H., Molina, L. T., Molina, M. J., Smith, T. J., and Garshick, E. (2004). Vehicle Traffic as a Source of Particulate Polycyclic Aromatic Hydrocarbon Exposure in the Mexico City Metropolitan Area. *Environ. Sci. Technol.* 38:2584–2592.
- Massoli, P., Kebabian, P.L., Onasch, T.B., Hills, F.B., and Freedman, A. (2010). Aerosol Light Extinction Measurements by Cavity Attenuated Phase Shift Spectroscopy (CAPS): Laboratory Validation and Field Deployment of a Compact Aerosol Extinction Monitor. *Aerosol Sci. Technol.* 44(6):428–435.
- Moosmuller, H., Chakrabarty, R. K., and Arnott, W. P. (2008). Aerosol Light Absorption and its Measurement: A Review, in *Annual Meeting of the Association-for-Aerosol-Research*, Karlsruhe, Germany, pp. 844–878.
- Moosmuller, H., Varma, R., and Arnott, W. P. (2005). Cavity Ring-Down and Cavity-Enhanced Detection Techniques for the Measurement of Aerosol Extinction. *Aerosol Sci. Technol.* 39:30–39.
- Murphy, D. M., Cziczo, D. J., Froyd, K. D., Hudson, P. K., Matthew, B. M., Middlebrook, A. M., Peltier, R. E., Sullivan, A., Thomson, D. S., and Weber, R. J. (2006). Single-particle Mass Spectrometry of Tropospheric Aerosol Particles. *J. Geophys. Res.—Atmospheres* 111: D23S32, doi:10.1029/2006JD007340
- Olfert, J. S., and Collings, N. (2005). New Method for Particle Mass Classification—the Couette Centrifugal Particle Mass Analyzer. *J. Aerosol Sci.* 36:1338–1352.
- Onasch, T. B., Jayne, J. T., Herndon, S., Worsnop, D. R., Miake-Lye, R. C., Mortimer, I. P., and Anderson, B. E. (2009). Chemical Properties of Aircraft Engine Particulate Exhaust Emissions. *J. Propulsion and Power* 25:1121–1137.
- Pagels, J., Khalizov, A. F., McMurry, P. H., and Zhang, R. Y. (2009). Processing of Soot by Controlled Sulphuric Acid and Water Condensation-Mass and Mobility Relationship. *Aerosol Sci. Technol.* 43:629–640.
- Paredes-Miranda, G., Arnott, W. P., Jimenez, J. L., Aiken, A. C., Gaffney, J. S., and Marley, N. A. (2009). Primary and Secondary Contributions to Aerosol Light Scattering and Absorption in Mexico City during the MILAGRO 2006 campaign. *Atmos. Chem. Phys.* 9:3721–3730.
- Park, K., Cao, F., Kittelson, D. B., and McMurry, P. H. (2003). Relationship Between Particle Mass And Mobility for Diesel Exhaust Particles. *Environ. Sci. Technol.* 37:577–583.
- Park, K., Kittelson, D. B., and McMurry, P. H. (2004). Structural Properties of Diesel Exhaust Particles Measured by Transmission Electron Microscopy (TEM): Relationships to Particle Mass and Mobility. *Aerosol Sci. Technol.* 38:881–889.
- Park, K., Dutcher, D., Emery, M., Pagels, J., Sakurai, H., Scheckman, J., Qian, S., Stolzenburg, M. R., Wang, X., Yang, J., and McMurry, P. H. (2008). Tandem Measurements of Aerosol Properties—A Review of Mobility Techniques with Extensions. *Aerosol Sci. Technol.* 42:801–816.
- Pettersson, A., Lovejoy, E. R., Brock, C. A., Brown, S. S., and Ravishankara, A. R. (2004). Measurement of Aerosol Optical Extinction at 532 nm with Pulsed Cavity Ring Down Spectroscopy. *J. Aerosol Sci.* 35:995–1011.
- Petzold, A., Schloesser, H., Sheridan, P. J., Arnott, W. P., Ogren, J. A., and Virkkula, A. (2005). Evaluation of Multiangle Absorption Photometry for Measuring Aerosol Light Absorption. *Aerosol Sci. Technol.* 39:40–51.
- Petzold, A., and Schonlinner, M. (2004). Multi-Angle Absorption Photometry—a New Method for the Measurement of Aerosol Light Absorption and Atmospheric Black Carbon. *J. Aerosol Sci.* 35:421–441.
- Ramanathan, V., and Carmichael, G. (2008). Global and Regional Climate Changes due to Black Carbon. *Nature Geo. Sci.* 1:221–227.
- Ramanathan, V., Crutzen, P. J., Kiehl, J. T., and Rosenfeld, D. (2001). Atmosphere – Aerosols, Climate, and the Hydrological Cycle. *Sci.* 294:2119–2124.
- Ramanathan, V., and Feng, Y. (2009). Air Pollution, Greenhouse Gases and Climate Change: Global and Regional Perspectives. *Atmos. Environ.* 43:37–50.
- Rypdal, K., Rive, N., Berntsen, T. K., Klimont, Z., Mideksa, T. K., Myhre, G., and Skeie, R. B. (2009). Costs and Global Impacts of Black Carbon Abatement Strategies. *Tellus Series B—Chem. Phys. Meteorol.* 61:625–641.
- Sakurai, H., Tobias, H. J., Park, K., Zarling, D., Docherty, S., Kittelson, D. B., McMurry, P. H. and Ziemann, P. J. (2003). On-Line Measurements of Diesel Nanoparticle Composition and Volatility. *Atmos. Environ.* 37:1199–1210.
- Schnaiter, M., Linke, C., Mohler, O., Naumann, K. H., Saathoff, H., Wagner, R., Schurath, U., and Wehner, B. (2005). Absorption Amplification of Black Carbon Internally Mixed with Secondary Organic Aerosol. *J. Geophys. Res.—Atmospheres* 110: D19204, doi:10.1029/2005JD006046
- Schwartz, S. E., and Buseck, P. R. (2000). Atmospheric Science—Absorbing Phenomena. *Sci.* 288:989–990.
- Schwarz, J. P., Gao, R. S., Fahey, D. W., Thomson, D. S., Watts, L. A., Wilson, J. C., Reeves, J. M., Baumgardner, D. G., Kok, G. L., Chung, S., Schulz, M., Hendricks, J., Lauer, A., Karcher, B., Slowik, J. G., Rosenlof, K. H., Thompson, T. L., Langford, A. O., Lowenstein, M., and Aikin, K. C. (2006). Single-Particle Measurements of Midlatitude Black Carbon and Light-Scattering Aerosols from the Boundary Layer to the Lower Stratosphere. *J. Geophys. Res.* 111:D16207, doi:10.1029/2006JD007076.
- Schwarz, J. P., Spackman, J. R., Fahey, D. W., Gao, R. S., Lohmann, U., Stier, P., Watts, L. A., Thomson, D. S., Lack, D. A., Pfister, L., Mahoney, M. J., Baumgardner, D., Wilson, J. C., and Reeves, J. M. (2008). Coatings and Their

- Enhancement of Black Carbon Light Absorption in the Tropical Atmosphere. *J. Geophys. Res.—Atmospheres* 113:D03203, doi:10.1029/2007JD009042.
- Schwarz, J. P., Spackman, J. R., Gao, R. S., Perring, A. E., Cross, E.S., Onasch, T. B., Ahern, A., Wrobel, W., Davidovits, D., Olfert, J., Dubey, M. K., Mazzone, C., and Fahey, D. W. (2010). The Detection Efficiency of the Single Particle Soot Photometer. *Aerosol Sci. Technol.* 44(8):612–628.
- Sedlacek, A. J. (2006). Real-Time Detection of Ambient Aerosols Using Photothermal Interferometry: Folded Jamin interferometer. *Review of Scientific Instruments* 77:064903.
- Sedlacek, A., and Lee, J. (2007). Photothermal Interferometric Aerosol Absorption Spectrometry. *Aerosol Sci. Technol.* 41:1089–1101.
- Seinfeld, J. H., and S. N. Pandis (2006). *Atmos. Chem. Phys.: From Air Pollution to Climate Change*. John Wiley & Sons, Inc., New York.
- Shiraiwa, M., Kondo, Y., Iwamoto, T., and Kita, K. (2010). Amplification of Light Absorption of Black Carbon by Organic Coating. *Aerosol Sci. Technol.* 44:46–54.
- Shiraiwa, M., Kondo, Y., Moteki, N., Takegawa, N., Sahu, L. K., Takami, A., Hatakeyama, S., Yonemura, S., and Blake, D. R. (2008). Radiative Impact of Mixing State of Black Carbon Aerosol in Asian Outflow. *J. Geophys. Res.—Atmospheres* 113: D24210, doi:10.1029/2008JD010546
- Slowik, J. G., Cross, E. S., Han, J. H., Davidovits, P., Onasch, T. B., Jayne, J. T., Williams, L. R., Canagaratna, M. R., Worsnop, D. R., Chakrabarty, R. K., Moosmuller, H., Arnott, W. P., Schwarz, J. P., Gao, R. S., Fahey, D. W., Kok, G. L., and Petzold, A. (2007a). An Inter-Comparison of Instruments Measuring Black Carbon Content of Soot Particles. *Aerosol Sci. Technol.* 41:295–314.
- Slowik, J. G., Cross, E. S., Han, J. H., Kolucki, J., Davidovits, P., Williams, L. R., Onasch, T. B., Jayne, J. T., Kolb, C. E., and Worsnop, D. R. (2007b). Measurements of Morphology Changes of Fractal Soot Particles using Coating and Denuding Experiments: Implications for Optical Absorption and Atmospheric Lifetime. *Aerosol Sci. Technol.* 41:734–750.
- Slowik, J. G., Stainken, K., Davidovits, P., Williams, L. R., Jayne, J. T., Kolb, C. E., Worsnop, D. R., Rudich, Y., DeCarlo, P. F., and Jimenez, J. L. (2004). Particle Morphology and Density Characterization by Combined Mobility and Aerodynamic Diameter Measurements. Part 2: Application to Combustion-Generated Soot Aerosols as a Function of Fuel Equivalence Ratio. *Aerosol Sci. Technol.* 38:1206–1222.
- Smith, J. D., and Atkinson, D. B. (2001). A Portable Pulsed Cavity Ring-Down Transmissometer for Measurement of the Optical Extinction of the Atmospheric Aerosol. *Analyst* 126:1216–1220.
- Stephens, M., Turner, N., and Sandberg, J. (2003). Particle Identification by Laser-Induced Incandescence in a Solid-State Laser Cavity. *Applied Optics* 42:3726–3736.
- Strawa, A. W., Castaneda, R., Owano, T., Baer, D. S., and Paldus, B. A. (2003). The Measurement of Aerosol Optical Properties using Continuous Wave Cavity Ring-Down Techniques. *J. Atmos. Oceanic Technol.* 20: 454–465.
- Zhang, R. Y., Khalizov, A. F., Pagels, J., Zhang, D., Xue, H. X., and McMurry, P. H. (2008). Variability in Morphology, Hygroscopicity, and Optical Properties of Soot Aerosols during Atmospheric Processing. *Proc. Natl Acad. Sci. USA* 105:10291–10296.